Published in final edited form as:

FASEB J. 2020 February ; 34(2): 3129–3150. doi:10.1096/fj.201902127R.

The Tripartite Interaction of Phosphate, Autophagy and αKlotho in Health Maintenance

Mingjun Shi[1], **Jenny Maique**[1], **Joy Shaffer**[1], **Taylor Davidson**[4], **Salwa Sebti**[2,4], **Álvaro F. Fernández**[2,4], **Zhongju Zou**[2,7], **Shirley Yan**[3], **Beth Levine**[2,4,5,7], **Orson W. Moe**[1,4,6,*], **Ming Chang Hu**[1,4,*]

[1]Charles and Jane Pak Center for Mineral Metabolism and Clinical Research, University of Texas Southwestern Medical Center, Dallas, TX, USA

[2]Center for Autophagy Research, University of Texas Southwestern Medical Center, Dallas, TX, USA

[3]Department of Pathology, University of Texas Southwestern Medical Center, Dallas, TX, USA

[4]Department of Internal Medicine, University of Texas Southwestern Medical Center, Dallas, TX, USA

[5]Department of Microbiology, University of Texas Southwestern Medical Center, Dallas, TX, USA

[6]Department of Physiology, University of Texas Southwestern Medical Center, Dallas, TX, USA

[7]Department of Howard Hughes Medical Institute, University of Texas Southwestern Medical Center, Dallas, TX, USA

Abstract

Aging-related organ degeneration is driven by multiple factors including the cell maintenance mechanisms of autophagy, the cytoprotective protein αKlotho, and the lesser known effects of excess phosphate (Pi), or phosphotoxicity. To examine the interplay between Pi, autophagy, and αKlotho, we used the *BK/BK* mouse (homozygous for mutant $Becn1^{F121A}$) with increased autophagic flux, and αKlotho-hypomorphic mouse (*kl/kl*) with impaired urinary Pi excretion, low autophagy, and premature organ dysfunction. *BK/BK* mice live longer than *WT* littermates, and have heightened phosphaturia from downregulation of two key NaPi cotransporters in the kidney. The multi-organ failure in *kl/kl* mice was rescued in the double mutant *BK/BK;kl/kl* mice exhibiting lower plasma Pi, improved weight gain, restored plasma and renal αKlotho levels, decreased pathology of multiple organs, and improved fertility compared to *kl/kl* mice. The beneficial effects of heightened autophagy from $Becn1^{F121A}$ was abolished by chronic high Pi diet which also shortened life-span in the *BK/BK;kl/kl* mice. Pi promoted beclin 1 binding to its

[*]**Address correspondence to:** Ming Chang Hu, M.D.; Ph.D., Charles and Jane Pak Center for Mineral Metabolism and Clinical Research, The University of Texas Southwestern Medical Center, 5323 Harry Hines Blvd., Dallas, TX 75390 USA, ming-chang.hu@utsouthwestern.edu, Or, Orson W. Moe, M.D., Charles and Jane Pak Center for Mineral Metabolism and Clinical Research, The University of Texas Southwestern Medical Center, 5323 Harry Hines Blvd., Dallas, TX 75390 USA, orson.moe@utsouthwestern.edu.

AUTHOR CONTRIBUTIONS

O.W.M, and M.C.H. designed and supervised the study; M.S., J.M., J.S., T.D., S.S., A.F.F., Z.Z., and S.Y. performed experiments; M.S., S.Y., B.L., O.W.M., and M.C.H. analyzed the data, O.W.M., and M.C.H. wrote the manuscript, O.W.M., B.L., and M.C.H. edited the manuscript.

negative regulator BCL2, which impairs autophagy flux. Pi downregulated αKlotho, which also independently impairs autophagy. In conclusion, Pi, αKlotho, and autophagy interact intricately to affect each other. Both autophagy and αKlotho antagonizes phosphotoxicity. In concert, this tripartite system jointly determines longevity and lifespan.

One Sentence Summary

Becn1 role in phosphate, αKlotho and lifespan

Keywords

Aging; autophagy; BCL2; beclin 1; fertility; αKlotho; longevity; NaPi cotransporter; phosphorus; phosphotoxicity

INTRODUCTION

Aging is an inevitable multi-organ deterioration initiated and accelerated by genetic, epigenetic, and environmental factors; among which is the lesser known factor of inorganic phosphate (Pi) intake in excess of the need of the organism (1–3). Excessive Pi intake is highly prevalent in the developed world (4). The ill effects of excess Pi at the cellular, organ, and whole organism levels are collectively termed “phosphotoxicity” (5–7). Compelling observational studies showed that phosphotoxicity is associated with reduced longevity in several species (8). In humans, high plasma Pi is an independent risk factor for cardiovascular disease (CVD) and mortality in patients with chronic kidney disease (CKD) and also in the general population (9). However, these associations albeit compelling, cannot prove casuality. In addition, the molecular mechanisms mediating phosphotoxicity in accelerating aging, and in initating and excerbating CVD are complex and multifactorial, and not understood (5, 10–12). Animal experiments showed that high Pi accelerates aging, and reduction of plasma Pi by either restriction of dietary Pi or induction of urinary Pi leak via genetic manipulation prolongs lifespan (10).

Autophagy is a universally conserved process employed by eukaryotic cells to degrade and reutilize the constituents of cytoplasm and organelles (13). Low autophagy is associated with shortened lifespan, and high autophagy prolongs life (14–16). Whether the detrimental effect of Pi on accelerating aging is related to autophagic flux has not been explored. We recently generated a mouse strain with a global knock-in of a F121A single amino acid substitution in the BH3 domain of mouse beclin 1 (*Becn1*^{F121A}), which impairs the ability of the negative regulator BCL2 to bind to beclin 1, consequently leaving beclin 1 to increase autophagic flux in multiple organs including brain, kidney, and muscle without alteration of endogenous levels of beclin 1 or/and BCL2 expression (15, 17). Mice harboring mutant *Becn1*^{F121A} have reduced cerebral amyloid accumulation, less cognitive decline, and increased survival when afflicted with Alzheimer’s-like disease (17), and less premature aging in mice with hypomorphic α*Klotho* allele (*kl/kl*) (15, 18) compared to Alzheimer mice and *kl/kl* mice respectively.

αKlotho was originally identified functionally as an aging suppressor due to the multi-organ premature degeneration in the homozygous hypomorph *kl/kl* mice (18) and a "longevity" phenotype in transgenic αKlotho overexpressing mice (*Tg-Kl* mice) (19). Transmembrane αKlotho is a co-receptor for fibroblast growth factor (FGF)23 (20–24), which is a Pi-regulating hormone promoting negative Pi balance (25). The ectodomain of membrane-anchored αKlotho is shed by secretases (26–28) into the circulation, and exerts FGF23-independent actions including anti-aging, anti-apoptosis, anti-senescence, and blockade of vascular calcification (29, 30). Soluble αKlotho, a cleaved extracellular domain of membrane-anchored αKlotho protein was proposed to also function as a deliverable soluble receptor for FGF23 in very high concentrations *in vitro* (31). The cellular and molecular mechanisms by which αKlotho deficiency initiates and/or promotes aging are not understood. Over-activity of insulin/insulin-like growth factor (32), plasminogen activator inhibitor-1 (33), low ectonucleotide pyrophosphatase/phosphodiesterase 1 (34), and high Pi (35) have all been proposed to be pathobiologic intermediates mediating the deleterious effects of αKlotho deficiency. The model to be tested is shown in Fig. 1A where defective autophagy, αKlotho deficiency, and phosphotoxicity all directly accelerate aging; in addition, each of these three factors also could modulate or amplify each other, thus secondarily contribute to aging. In this study, we used genetic and pharmaceutic approaches to manipulate autophagy activity, αKlotho levels, and dietary Pi content to examine the inter-relationships of these three factors and how they converge to acceleate aging (Fig. 1A).

MATERIALS AND METHODS

Mice and murine strains

All animal work was conducted strictly following the Guide for the Care and Use of Laboratory Animals by the National Institutes of Health and was approved by the Institutional Animal Care and Use Committee at the University of Texas Southwestern Medical Center. Wild type (*WT*) *129 S1/SVlmJ* (*129sv*) mice were purchased from Jackson laboratory (Bar Harbor, ME, USA). *WT* mice were housed in a temperature-controlled room (22.0±0.2 °C) with a 12:12 hour light-dark cycle and were given *ad libitum* access to tap water and allowed free access to standard rodent chow (Teklad 2016, Harlan, Madison, WI) unless stated otherwise. Equal male and female animals were used. Usually 10–12 week-old mice were used unless specifically indicated. Mouse lines were cross-mated with *WT 129sv* mice for more than 10 generations and genotyped with standard PCR protocols described in the previous publications: heterozygous αKlotho hypomorphic (*kl/+*) mouse (36), transgenic mouse with αKlotho overexpression (*Tg-kl*) (36), GFP-LC3 reporter (*LC3*) mouse (36), homozygous Becn1F121A knock-in (*BK*) mouse (17), heterozygous global Becn1 knockout ($Becn1^{+/-}$) mouse (37), homozygous BCL2AAA knock-in ($Bcl2^{AAA}$) mouse (38). *BK/WT;kl/+* mouse line was generated by cross-mating *BK* mice with *kl/+* mice and *BK/BK;kl/kl* mouse line was generated when *BK/WT;kl/+* mice were cross-mated with *themselves*.

Cell culture and cell lines

Two types of cell lines were used. (1) Opossum kidney PTH responsive cells (OKP cells), a proximal tubule–like epithelial cell line, were grown on culture dishes or on insert filters

with 0.4 μm pores (Transwell Inserts, Corning Incorporated). Cells grown on culture dishes were collected for immunoblot and culture media for lactic acid dehydrogenase (LDH) assay to evaluate cell injury. Cells grown on insert filters were fixed for immunocytochemistry or transmission electron microscopy. (2) Human embryonic kidney cells (HEK-293) lacking a native Na-dependent Pi cotransporter type II a (NaPi-2a) and NaPi-2c protein expression, were transiently transfected with human NaPi-2a and NaPi-2c plasmids with Lipofectamine 2000 (Invitrogen, Carlsbad, CA) for characterization of newly generated NaPi-2a and 2c antibodies.

High phosphate diet

High Pi rodent chow (2.0% w:w) was purchased from Harlan company (Teklad 08020, Harlan, Madison, WI) and used to examine the effect of high Pi diet on autophagic flux and αKlotho expression.

Recombinant αKlotho protein supplementation

Recombinant αKlotho protein containing the ectodomain of mouse αKlotho (amino acid number 31–982) with C-terminal V5 and 6xHis tags was generated in our laboratory as described (39, 40). For the *in vivo* experiments, recombinant αKlotho protein (0.3 mg/kg body weight) or vehicle (normal saline) was given for 4 weeks via ALZET® 1004 osmotic minipumps (DURECT Corporation, Cupertino, CA).

In vivo administration of autophagy modulators

To modulate autophagy activity in mice, rapamycin (LC Laboratories, Woburn MA) and chloroquine (Sigma-Aldrich, St. Louis, MO) were prepared as previously reported (15, 36, 41), and were intraperitoneally given for 4 weeks via ALZET® 1004 osmotic minipumps (DURECT Corporation, Cupertino, CA) at doses of: rapamycin 28 mg/Kg, and chloroquine 50 mg/Kg respectively.

Blood, urine, and kidney samples collection

At predetermined times, 24-hour urine was collected in individual metabolic cage. The mice were anesthetized with isoflurane and blood samples were collected in heparinized tubes, centrifuged at 3,000 × g for 5 min at 4°C, and plasma was separated and stored at −80°C until analysis. At termination, mice were sacrificed under anesthesia, and the kidneys were isolated and sliced. One slice was fixed with 4% paraformaldehyde and embedded in a paraffin block for histological and immunohistological studies; the remaining renal tissue was snap-frozen in liquid N_2 and stored at −80°C until RNA or protein extraction.

Plasma and urine chemistry was analyzed using a Vitros Chemistry Analyzer (Ortho-Clinical Diagnosis, Rochester, NY). Plasma and urine creatinine concentrations were measured using a P/ACE MDQ Capillary Electrophoresis System and photodiode detector (Beckman-Coulter, Fullerton, CA) at 214 nm (36, 39).

In vivo and *in vitro* administration of Tat-beclin 1 peptides

Tat-beclin 1 11 peptides (TB-11) (YGRKKRRQRRR-GG-VWNATFHIWHD) and Tat-Scrambled peptides (TB-Sc) (YGRKKRRQRRR-GG-WNHADHTFVWI) were synthesized

by the University of Texas Southwestern Protein Technology Center as reported previously (42, 43). To examine the effect of beclin 1 on modulation of Pi metabolism in mice, we intraperitoneally injected TB-11 or TB-Sc to *LC3* mice (2 mg/kg daily for 4 weeks), followed by intraperitoneal chloroquine injection (50 mg/kg) 4 hours prior to sacrifice. Twenty-four-hour urine was collected, blood drawn, and Kidney tissues harvested.

To examine the protective effect of beclin 1 on phosphotoxicity in cultured cells, TB-11 or TB-Sc (10 μM for 24 hours), OKP cells were incubated with normal (0.96 mM) or high (3.0 mM) Pi culture media. Culture media were collected for LDH determination and cells harvested for the evaluation of autophagy activity.

Measurement of plasma αKlotho

Soluble αKlotho was determined by immunoprecipitation-immunoblot as described (12, 44, 45). Intact parathyroid hormone (PTH) was quantified by ELISA (Alpco, Salem, NH); 1,25-$(OH)_2D$ by EIA using (Immunodiagnostic Systems, Scottsdale, AZ); and C-terminal FGF23 by ELISA (Immutopics, San Clemente, CA) following manufactures' instructions.

Plasmids

The GFP-LC3 plasmid was kindly provided by Dr. Mizushima N (Tokyo Medical and Dental University, Tokyo, Japan). Its information was described in our previous publications (36, 41). Full length human NaPi-2a and NaPi-2c were subcloned and inserted with *XhoI* and *SacII* restriction enzymes into eGFP-N3 vector (Clontech, Palo Alto, California). All sequences were confirmed by the sequencing Core at UT Southwestern Medical Center.

Fluorescent microscopy and transmission electron mcroscopy

For the study of high Pi effect on autophagic flux with fluorescent microscopy, OKP cells were seeded on insert filters or on culture dishes, and transiently transfected with GFP-LC3 plasmid as described previously (15, 36, 41). One day after transfection, cells were treated with culture media containing 0.96, 2.0 or 3.0 mM Pi for 24 hours respectively.

OKP cells were seeded, grown on 0.4 μm pores Snapwell™ Insert filters (Corning Incorporated Life Sciences, Tewksbury, MA), and fixed with 2.5% glutaraldehyde at 4°C for 2 hours. The filters (with cells) were cut to 1×1 mm pieces, embedded in 3% agarose, post-fixed in 1% osmium tetroxide, and embedded in Resin812. Ultrathin sections were cut by using a Microtome Leica Ultracut R (Leica Microsystems Inc, Buffalo Grove, IL, USA). The sections were stained with 1% uranyl acetate and Reynold's lead citrate. The sections were examined and photographed by using a Jeol 1200 EX transmission electron microscope (Jeol Ltd., Akishima, Japan) as described (36, 46). Twenty cells in each slide were observed and autophagosomes and multilamellar bodies (MLBs) were counted based on typical morphologic features by one independent investigator blinded to study protocol.

Antibodies

The following antibodies were used for immunoblotting and/or immunohistochemistry: mouse monoclonal anti-beclin 1 (Santa Cruz Biotechnology, Santa Cruz, CA), mouse monoclonal anti-BCL2 (Santa Cruz Biotechnology, Santa Cruz, CA), rat monoclonal anti-

Klotho antibody (KM2076) (TransGenics, Kobe, Japan), rabbit polyclonal anti-LC3 antibody (Novus Biologicals, Littleton, CO), mouse monoclonal antibody against α-SMA (Sigma Aldrich, St. Louis, MO), mouse monoclonal anti-p62/SQSTM1 antibody (Abnova, Taiwan), mouse monoclonal antibody against β-actin (Sigma Aldrich, St. Louis, MO), and mouse monoclonal antibody against glyceraldehyde-3-phosphate dehydrogenase (GAPDH) (Sigma Aldrich, St. Louis, MO). Rabbit polyclonal antibodies against human NaPi-2a or NaPi-2c were made by Yenzym Antibodies, LLC (San Francisco, CA). The peptide sequences for immunizing rabbit for NaPi-2a and NaPi-2c are human NaPi-2a peptide (77–96, CKLALEEEQKPESRLVPKLRQ) or human NaPi2c peptide (579–599, KATTKEAYCYENPEILASQQL) respectively and the specificity of anti-serum was confirmed with kidney tissues from NaPi-2a or 2c knockout mice. Secondary Abs coupled to horseradish peroxidase for immunoblotting, or to FITC, Alexa Fluor, or Cy5, and Syto 61 red fluorescent nuclear acid for immunohistochemistry were purchased from Molecular Probes/Invitrogen (Molecular Probes Inc., Eugene, OR).

Kidney histology and histopathology

Kidney tissues were fixed in 4% paraformaldehyde for 16 hours at 4 °C, and 4 μm sections of paraffin embedded kidney tissues were stained with Hematoxylin and Eosin (H&E) and Trichrome (TC). To evaluate renal fibrosis, TC stained kidney sections were examined and photographed by two investigators blinded to the experimental protocol. The fibrotic area and fibrosis intensity were quantified with Image J program with established methods (40, 41, 47).

Immunohistochemistry and immunoblotting

Four μm sections of paraffin-embedded kidney were subjected to immunohistochemistry following established protocols (36, 40, 41, 47). Total kidney lysate covering all kidney zones were prepared and subjected to SDS-PAGE as described (40, 47).

Assessment of cardiac fibrosis and hypertrophy

Paraffin-embedded heart sections were stained with Trichrome to assess fibrosis. Images were then scanned with Zeiss laser confocal scanning microscope (Carl Zeiss Micro-Imaging, Inc. Thornwood, NY), and analyzed using the Image J program (12, 40, 48). The scar ratio is the area of collagen deposition divided by the total area of cardiac musculature. To measure surface area of cardiomyocytes in the hearts, heart sections were labeled with wheat germ agglutinin (WGA) conjugated to Alexa Fluor 555 (ThermoFisher Scientific, Eugene, OR). Image J software (NIH) was used to quantify cross-sectional cell surface area along the mid-chamber free wall of left ventricle based on WGA-positive staining (12, 40, 48).

Von Kossa staining and calcium content measurement

The aorta was stained for calcification with Von Kossa (45). Tissue sections were incubated with 1% silver nitrate solution under ultraviolet light for 30 minutes followed by incubation with 5% sodium thiosulfate for 10 minutes to remove the un-reacted silver. Aortic sections were counterstained with nuclear fast red, photographed blindly by two investigators using

Axioplan 2 Imaging (Carl Zeiss MicroImaging, Inc. Thornwood, NY). The calcium concentration in tissues was measured using the o-cresolphthalein complexone method (Sigma-Aldrich, St. Louis, MO) (45, 49). The calcium content (μg/mg protein) was quantified by normalization to protein concentration determined by Bradford protein assay.

Quantitative polymerase chain reaction (qPCR)

For PCR, total RNA was extracted by RNAeasy kit (Qiagen, Germantown, MD) from mouse kidneys. Complimentary DNA (cDNA) was generated with oligo-dT primers using SuperScript III First Strand Synthesis System (Invitrogen, Carlsbad, CA) according to manufacturer's protocol. Primers of mouse α*Klotho* and *cyclophilin* used for qPCR and conditions were shown in our previous publications (40, 45). Data are expressed at amplification number of $2^{-\Delta\Delta Ct}$ by normalization of *cyclophilin* and comparison to controls.

Statistical analysis

Survival rates during the survival study was assessed using the log rank test to compare the differences in Kaplan-Meier survival curves. Data are expressed as means ± S.D. unless otherwise specified. Analysis was performed with Sigma Plot 13.0 software (Systat Software, Inc. San Jose, CA). As appropriate, statistical analysis was performed using unpaired *Student-t*-test, or one-way or two-way analysis of variance (ANOVA) followed by Student-Newman-Keuls *post hoc* test when applicable as specified. A value of $P \leq 0.05$ was considered statistically significant.

RESULTS

The tripartite interacting model we tested is shown in Fig. 1A, depicting how each of the three factors can individually and directly influence aging but also interact, modulate, and amplify each other. These relationships will be tested individually and in concert with *in vivo* and *in vitro* models.

Autophagy and phosphate: high autophagy activity is associated with low plasma Pi and high phosphaturia

The first arm of Fig. 1A we tested was the influence of autophagy on Pi homeostasis. Before full embarkment of experiments, we first ensured that we can fully explore "phosphate sensitivity" of mouse strains to enable testing of phosphotoxicity. We crossed the *BK/BK* mouse (homozygous for the mutant $Becn1^{F121A}$) onto a *129sv* background of the *kl/kl* mice. The rationale is based on our personal experience and knowledge of the relative resilience of the C57BL6 mice to phosphotoxicity. The new line of *BK/BK* mice had a mixed *C57BL/6;129sv* background, but maintained the same features of high autophagic flux (Supplementary Fig. 1A–C) demonstrated by higher ratios of LC3II/I, as previously reported for the *BK/BK* mice in *C57BL/6* background (15, 17).

To study the role of autophagy in Pi homeostasis, we measured Pi in *BK/BK* mice and found that they had lower plasma Pi compared to *WT* litermates (Fig. 1B left panel) and higher urinary fractional excretion of Pi (FE_{Pi}), indicating heightened renal excretion accounting for the lower plasma Pi (Fig. 1B right panel). Pi is regulated by the kidney in a filtration-

reabsorption mode, and Pi reabsorpiton is mediated by type II Na^+-dependent Pi cotransporters (NaPi) including NaPi-2a and 2c in the renal proximal tubules, and phosphaturia is usually achieved by downregulation of Pi reabsoption by NaPi-2a and −2c (6, 24, 50). Due to the variable and nondependable quality of commerical antibodies, we generated and validated new rabbit polyclonal antibodies against NaPi-2a and NaPi-2c ourselves for this project (Supplementary Fig. 2) and used these two new antibodies to measure the expression of NaPi-2a and NaPi-2c in *BK/BK* mice. We found that *BK/BK* mice had lower NaPi-2a and 2c protein expression in the kidney (Fig. 1C) and in apical membrane of renal proximal tubules of *BK/BK* mice (Fig. 1D and Supplementary Fig. 3), indicating that increased autophagy downregulates NaPi's expression in renal tubules to decrease Pi reabsorption and promote phosphaturia.

Autophagy and Klotho effects on phosphate: level of autophagy activity is positively correlated with αKlotho levels, and both autophagy and αKlotho modulate plasma Pi

We next explored the more complex tripartite relationship between plasma Pi, autophagy activity, and αKlotho levels. Since plasma Pi is inversely associated with lifespan (8), we measured plasma Pi in several mouse lines manipulated to have low, normal or high autophagy acitivity and also low, normal, or high αKlotho, which is a known phosphaturic substance (24). Both the *BK/BK* and *Tg-Kl* mice with high autophagy and αKlotho respectively, had higher FE_{Pi} and lower plasma Pi compared to *WT* (Fig. 1E). Reduced autophagy was achieved by two methods. We used the haploinsufficient $Becn1^{+/-}$ mice with reduced Beclin 1 and autophagic flux (37, 51), and the $Bcl2^{AAA}$ mice with knock-in of mutant BCL2 at three phosphorylation residues in the non-structured loop region, T69A, S70A and S84A (homologous to human S87A) which confers constitutive BCL2 inhibition of Beclin 1 (38). Regardless of how autophagy flux was decreased, both $Becn1^{+/-}$ and $Bcl2^{AAA}$ mice had higher plasma Pi and lower FE_{Pi} compared to *WT* mice (Fig. 1E). At one extreme end is the *kl/kl* mouse, which has the highest plasma Pi and lowest FE_{Pi} (Fig. 1E). The important finding is that in contrast to the severe hyperphosphatemia in *kl/kl* mice, plasma Pi was remarkably reduced in the 10-week-old double *BK/BK;kl/kl* mice which surprisingly approaches that of *WT* mice of the same age indicating rescue of the severe *kl/kl* phosphste-retaining phenotype by activation of autophagy flux (Fig. 1E).

To further examine the relationship between beclin 1 activity, plasma Pi and αKlotho status, we measured autophagic flux and αKlotho levels in the kidney and compared them with those in *kl/kl* mice (extremely low αKlotho) (18) and a transgenic mouse line with global overexpression of αKlotho by a universal promoter (*Tg-Kl* mice) resulting in modestly elevated αKlotho (1.5x wild type) and lower plasma Pi (24, 32). Two mouse lines with low beclin 1 activity ($Becn1^{+/-}$ and $Bcl2^{AAA}$) had higher plasma and renal aKlotho levels compared to mouse line with high beclin 1 activity (*BK/BK*) (Fig. 1F, G). Thus, Beclin 1 activity is negatively correlated with plasma Pi levels and positively associated with FE_{Pi} levels (Fig. 1E), and plasma and renal αKlotho levels (Fig. 1F, G).

Autophagy and Klotho: high beclin 1 activity restores αKlotho in αKlotho hypomorphic mice

The next arm of the tripartite model to be tested is whether autophagy is upstream of and modulates αKlotho. Plasma Pi is a downstream surrogate for systemic αKlotho bioactivity. To fully define the time profile of changes in plasma Pi, we longitudinally followed plasma Pi in mice with all 4 genotypes (*kl/kl, kl/kl;BK/BK, WT, BK/BK*) from weaning to 120 weeks of life. In parallel with the dramatic elongation of lifespan of the *kl/kl* mice by increasing beclin 1 activity (Fig. 2A), *BK/BK;kl/kl* mice sustainably gained body weight (Fig. 2B) even though they were still smaller than *WT* littemates at same age, and had decreased levels of plasma Pi (Fig. 2C), which had never been observed in *kl/kl* mice. Interestingly, *BK/BK;kl/kl* mice had increased autophagy flux in the kidney compared to *kl/kl* mice although the flux was lower than that of *BK/BK* mice at age of 6 or 10 weeks (Fig. 2D), indicating that one can increase autophagy activty in the *kl/kl* mice by elevation of beclin 1 activity.

To study the change in plasma αKlotho in *BK/BK;kl/kl* mice, we longitudinally followed plasma αKlotho in all of 4 genotypes from weaning to 10 weeks after birth. Not suprisingly, with a dysfunctional αKlotho promoter (the primary lesion in *kl/kl* mice), plasma and renal αKlotho levels remained undetectable at 6 weeks in the *BK/BK;kl/kl* mice (Fig. 2E, F). However, note that αKlotho protein was actually weakly detectable in the kidney and plasma, and higher than that of *kl/kl* mice by 8 weeks of age (Supplementary Fig. 4). Surprisingly by 10 weeks, αKlotho protein levels were unequivocally appreciable in both plasma and the kidney (Fig. 2E, F) albeit still lower than *WT* mice. Notably, αKlotho levels in the kidney of *BK/+;kl/kl* mice bearing only one copy of the activated *becn1* mutant, were lower than those in *BK/BK;kl/kl* mice at 12 weeks old (Supplementary Fig. 5), suggesting that beclin 1-induced restoration of αKlotho is of dose-dependence either directly or via better maintenance of Pi homoestasis.

End organ phenotype: high beclin 1 activity alleviates cardiac pathology in αKlotho hypomorphic mice

If the individual components of the tripartitie model (Fig. 1A) interact with each other to affect health maintenance, there should be detectable end organ effects as we manipulate each of the components. We demonstrated that high autophagy rescues αKlotho deficiency and positions Pi homeostasis away from phosphotoxicity. Here we examined the effect of high beclin 1 activity on the cardiovascular system, because cardiomyopathy and vascular calcification are two cardinal manifestions and prinicpal contributors to the short lifespan in *kl/kl* mice (52, 53), and in humans with CKD who classically have low αKlotho and high serum Pi levels (12, 54). *BK/BK;kl/kl* mice had basically normal histology of the cardiovascular system at 10 weeks of age (Fig. 3A – D). Vascular calcification in aortic roots, and cardiac hypertrophy and fibrosis normally present in the *kl/kl* mice were significantly attenuated in *BK/BK;kl/kl* mice compared to *kl/kl* mice (Fig. 3A – D), indicating that high beclin 1 activity ameliorates cardiovascular abnormalities prominently present in *kl/kl* mice.

End organ phenotype: high beclin 1 activity restores reproductive function in both male and female αKlotho hypomorphic mice

Restoration of αKlotho level, abrogation of phosphotoxicity, and improvement of cardiovascular outcome are pivotal results of heightened autophagy. Another important end organ effect of the trinity of modulators is reproductive health. Infertility and early loss of reproduction are characteristics of the *kl/kl* mice and so are features of aging (18, 55). Both male and female *kl/kl* mice stopped growing after weaning with small body mass (Supplementary Fig. 6A). Male *kl/kl* mice had testicular atrophy with less spermatids and no spermatocytes release into the lumen of seminiferous tubules. Female *kl/kl* mice had uterine atrophy and ovarian atrophy (Supplementary Fig. 6B, C). There was either complete absence or much reduced follicles and interstitial infiltration in female *kl/kl* mice. Interestingly, both male and female *BK/BK;kl/kl* mice had near normal body size and normal morphogy (Supplementary Fig. 6B) and histology (Supplementary Fig. 6C) of testis and ovary respectively compared to male and female *WT* mice, and also had intact reproduction (data not shown) suggesting that infertility in *kl/kl* mice was rescued by high beclin 1 activity. Moreover, both male and female *BK/+;kl/kl* mice were fertile after cross-mating (data not shown), indictating that beclin 1^{F121A} exerts a dominant effect, and one copy of $Becn1^{F121A}$ is able to protect the murine reproductive system from αKlotho deficiency and phosphotoxicity.

End organ phenotype: high beclin 1 activity alleviates renal abnormalities in the αKlotho hypomorphic mice

In addition to the heart and reproductive organs, another important end organ phenotype in αKlotho deficiency is the heightened propensity for kidney disease. Trichrome-stained kidney sections were used to examine the effect of high autophagy activity on renal histology. The renal fibrosis characteristically seen in *kl/kl* mice was remarkably decreased in *BK/BK;kl/kl* mice (Supplementary Fig. 7 and Fig. 3E). The fibrotic marker α-SMA in the kidney was reduced in *BK/BK;kl/kl* mice (Fig. 3F) compared to *kl/kl* mice. Ectopic calcification which is prominently present in the kidney of *kl/kl* mice was not even detectable in *BK/BK;kl/kl* mice (Fig. 3G).

Early pharmacologic modulation of autophagy activity influences murine growth

To confirm that the high beclin 1 activity-associated prevention of premature death and organ and tissue degeneration is directly attributable to upregulation of autophagy flux, we used an alternative mode of pharmacologic activation of autophagy to treat *kl/kl* mice with rapamycin, a known autophagy inducer, for 4 weeks (Fig. 4A). The rapamycin-treated *kl/kl* mice had slightly higher body weight gain, which was similar to, but less than αKlotho-treated *kl/kl* mice. In contrast, chloroquine (CQ), an autophagy suppressor, exaggerated the slow growth (Fig. 4B). Moreover, rapamycin-treated *kl/kl* mice had lower levels of plasma Pi, which were similar to those in αKlotho-treated *kl/kl* mice, while CQ-treated mice had higher levels of plasma Pi than vehicle-treated *kl/kl* mice (Fig. 4C). Although a short period of rapamycin treatment did not increase renal αKlotho protein expression (Fig. 4D), renal fibrosis was significantly attenuated in *kl/kl* mice treated with either rapamycin or αKlotho, but worsened in CQ-treated *kl/kl* mice (Fig. 4E). Therefore, the high autophagy-induced

improvement of renal abnormalities in *kl/kl* mice may result at least in part from improved Pi homeostasis prior to changes in αKlotho levels.

Phosphate effect on autophagy: high Pi diet reverses high beclin 1 activity-induced improvement of growth

If improved Pi homeostasis in *BK/BK* mice is mediating the phenotypic rescue in *kl/kl* mice, one should be able to overwhelm the beneficial effect with Pi loading. We therefore fed mice with the 3 genotypes (*WT, BK/BK,* and *BK/BK;kl/kl*) with high Pi diet starting at 6-weeks old for a duration of 6 weeks. From our experience, *kl/kl* mice are very fragile, intolerant to high Pi, and will universally succumb, so they were not studied. High Pi diet decreased mouse growth, which was more appreciable in *BK/BK;kl/kl* mice than the *WT* and *BK/BK* mice (Fig. 5A and B), indicating that the beneficial restoration of growth by high autophagy was abolished by high Pi diet. The 12-week survival of *BK/BK;kl/kl* mice was 92% under normal Pi diet, which was reduced to 52% after 6-weeks of high Pi feeding (Fig. 5C). The low survival rate was associated with higher plasma Pi (Fig. 5D), low autophagy flux in the kidney (Fig. 5E), and low endogenous αKlotho (Fig. 5F). The reduction in mortality in *BK/BK;kl/kl* mice previously observed was dramatically reversed by high Pi diet. Note that *BK/BK* mice were more resistant to phosphotoxicity under the high Pi diet than *WT* mice because *BK/BK* mice maintained relatively normal plasma Pi (Fig. 5D), higher autophagy flux in the kidney (Fig. 5E), and higher αKlotho expression in the kidney (Fig. 5F).

High Pi diet blunts the high beclin 1 activity-induced improvement of renal and cardiac phenotypes in αKlotho hypomorphic mice

In addition to poor growth (Fig. 5A to C), higher plasma Pi levels (Fig. 5D), lower autophagic flux (Fig. 5E), and lower αKlotho (Fig. 5F) in the kidney after 6-week high Pi dietary intake, were associated with higher α-SMA expression in the kidney (Fig. 6A) and more renal fibrosis (Fig. 6B) in *BK/BK;kl/kl* mice compared to *WT* or *BK/BK* mice, suggesting that *BK/BK;kl/kl* mice are more sensitive to phosphotoxicity.

Six weeks of high dietary Pi challenge also induced cardiac fibrosis (Fig. 6C) and hypertrophy (Fig. 6B), and upregulated markers of hypertrophy (α-actinin) and fibrosis (α-SMA) in *WT* mice (Fig. 6E), which were similar to our previous findings (12, 40). Interestingly, *BK/BK* mice were more resistant, and the *BK/BK;kl/kl* mice were more susceptible to cardiac phosphotoxicity.

We examined the effect of high Pi diet on parameters of mineral metabolism in *BK/BK;kl/kl* mice and compared these changes in *BK/BK;kl/kl* mice with other genotypes. In addition to decreasing plasma and renal αKlotho (Fig. 5F and Table 1), 6-week of high Pi diet increased plasma FGF23, and slightly elevated plasma 1,25-$(OH)_2$-vitamin D (1,25-$(OH)_2$-D) in both *WT,* and *BK/BK;kl/kl* mice but not in *BK/BK* mice. Clearly there were more severe changes in low αKlotho, high plasma FGF23 and 1,25-$(OH)_2$-D induced by high Pi diet in *BK/BK;kl/kl* mice compared to *WT* and *BK/BK* mice.

High Pi downregulates autophagy flux and αKlotho

To complete the study of all the arms in the trinity in Fig. 1A, we explored if high Pi diet modifies autophagic flux in kidneys. Mice with normal kidney function consuming high Pi diet for 2 weeks did not have significantly higher plasma Pi (Fig. 7A left panel) likely due to the appropriate compensatory urinary Pi excretion (Fig. 7A right panel). But despite the lack of detectable hyperphosphatemia, Pi load *per se* led to lower autophagic flux (Fig. 7B, C) and lower renal αKlotho protein and mRNA (Fig. 7B, and Supplementary Fig. 9). In addition, high Pi-fed mice had increased beclin 1/BCL2 complex (Fig. 7D). Taken together, high Pi diet not only markedly downregulated αKlotho, but also decreased autophagic flux in the kidney, suggesting that all of these three factors may interplay in a highly regulated network.

It is difficult to draw definitive conclusions within the complexity of the whole organism due to the multiple possible intermediate mediators. To address the direct effect of high Pi on autophagic flux, we proceeded to OKP cells, a renal epithelial cell line (36). High Pi media significantly reduced autophagy flux (Fig. 7E, F) and induced cell injury demonstrated by higher levels of LDH in the media, which was Pi concentration-dependent (Supplementary Fig. 7). Both LC3-I and LC3-II proteins were increased as well as elevation of p62 and diminution of LC3 punctas (Fig. 7E, F), which suggest incomplete block of autophagic flux when cells are exposed to high Pi. Moreover, high Pi stabilized the beclin 1/BCL2 complex in cells (Fig. 7G). Electron photomicrographs showed significantly fewer autophagosomes and autolysosomes, but massive accumulation of MLBs delimited by a single layer of plasma membrane (56) in cells treated with high Pi media compared to normal Pi treated cells. Notably, we cannot find a single MLB in cells treated with normal Pi media despite extensive searching (Fig. 7H). Accumulation of MLBs in the tissues is generally attributable to insufficient degradation of deposited MLBs (57, 58). It is conceivable that high Pi downregulates autophagy flux probably through two mechanisms: insufficient biogenesis of autophagosomes due to stabilizing beclin 1/BCL2 complex, and incapacity of autolysosomes processing and recycling.

Beclin 1 peptides upregulates autophagy flux and protects against phosphotoxicity

Tat-beclin 1 11 (TB-11) is an autophagy-inducing peptide comprising 11 amino acids derived from beclin 1 diglycine linked to the HIV Tat protein. These peptides are in the retro-inverso D-configuration (42, 43). TB-11 is a shorter peptide with higher penetrance into cells than, but has similar bioactivity as Tat-beclin 1 (18 amino acids), (42, 43, 59). Beclin 1 peptide is an active functional unit of beclin 1 protein (42, 43, 59). To test beclin 1 effect on prevention against phosphotoxicity, we first determined TB-11 effect on Pi metabolism *in vivo* and found that 4-week TB-11 significantly reduced plasma Pi probably through induction of urinary Pi leak (Fig. 8A). To further confirm TB-11 effect on autophagy activity *in vivo*, we explored the profile of autophagy flux in the kidneys after TB-11. TB-11 upregulated αKlotho expression increased the ratio of LC3II/I and LC3II and reduced p62 in the kidney (Fig. 8B) as well as elevation of LC3 punctas in renal tubules (Fig. 8C).

We next used the OKP cell line as *in vitro* model to test direct protective action of TB-11 against phosphotoxicity. After co-incubation of OKP cells with TB-11 and high Pi (3.0 mM) for 24 hours, we found higher autophagic flux as demonstrated by higher LC3 II/I, LC3 II and lower p62 expression compared to TB-Sc (Fig. 8D). Importantly, LDH release induced by high Pi was significantly reduced compared to TB-Sc (Fig. 8E), supporting cytoprotection by TB-11 against phosphotoxicity.

DISCUSSION

This is the first demonstration of an interactive relationship of autophagy (beclin 1), αKlotho, and Pi, and how the three can act individually or via modulating each other in controlling health and longevity (Fig. 1A). We propose that high Pi, low αKlotho, and low autophagy are independent contributors to multi-organ degeneration with reciprocal mutual amplifications. High Pi downregulates autophagic flux via increased beclin 1/BCL2 complex formation, and suppression of αKlotho. Either high or low αKlotho further exacerbate low autophagic flux, constituting a triple interactive and self-amplifying loop. Low Pi, increased autophagy, and αKlotho, function independently and cross-regulate each other to synergistically retard aging and prolong lifespan. Disruption of one or all three can have undesirable consequence on aging and health (Fig. 1A). A few salient features of the current dataset deserve discussion.

Autophagy affects phosphate homeostasis through induction of phosphaturia

The role of autophagy in prevention of aging in the kidney and the heart has been documented (15, 36), but the underlying mechanisms have not been deciphered. Normal Pi homeostasis contributes to maintenance of lifespan and retardation of degeneration in multiple organs including the heart and kidney (10, 12, 60). Genetic and dietary normalization of blood Pi rescues many phenotypes including ectopic calcification in the kidney, heart and aorta, cardiac abnormalities, early death, infertility in aging animals (8, 10, 61). The current study provides *in vivo* evidence that high beclin 1 activity induces phosphaturia via downregulation of renal NaPi-2a and 2c expression, and the negative Pi balance consequently upregulates αKlotho, retards aging, and ameliorates tisues and organs degeneration to better maintain function of the cardiovascular, reproductive and renal systems.

The conclusion was fortified by finding of similar results with pharmcologic manipulation of autophagy *in vivo*. Even a short period of rapamycin treatment made *kl/kl* mice gain weight, lowered their plasma Pi, but without detectable change in αKlotho, while CQ treatment had the opposite effect on *kl/kl* mice. The reduction of plasma Pi by rapamycin or other mTOR inducers has been reported in humans (62) and animals (63, 64) but the effect on NaPi2a expression has been less consistent (65). In addition, whether the rapamycin-induced phosphaturia is autophagy-dependent or/both autophagy-independent is unknown. The current dataset proves that rapamycin could induce phosphaturia and prevent phosphotoxicity via upregulation of autophagy flux as one of its mechanisms, which is supported by the animal experiment in the *BK* mice and TB-11-treated *WT* mice. The

contribution of non-autophagy-dependent effects of rapamycin remains plausible and deserves future exploration.

Improvement of Pi metabolism might be a sufficient driving force to enhance autophagy and longevity. The decreased plasma Pi and increased urinary Pi excretion in mice after adminstration of TB-11, the active and functional peptide of beclin 1 futher proves the concept that high autophagy in the kidney promotes negative Pi balance. The restored body growth and reduced mortality in *BK/BK;kl/kl* mice was abolished by high Pi diet further supporting the phosphotoxic effect on accelerating aging. The *in vitro* experiment with TB-11 showing lower LDH release from proximal tubule cells cultured in high ambient Pi provides direct evidence that beclin 1 is cytoprotective against phosphatoxicity.

The role of autophagy in regulation of renal transport (66, 67) including water (68, 69), glucose (70), cysteine (71) and other electrolytes (72) have been reported. The current manuscript provides new data linking autophagy with phosphate transport in the renal tubules. Autophagy might modulate NaPi2a/2c endocytosis via the canonical mechanisms of modification of trafficking (73–76) to control renal tubular Pi reabsorption. Alternatively, there can be novel mechanisms by which autophagy can regulated NaPi protein distribution and activity.

αKlotho modulates phosphate metabolism and autophagy activity

Despite the fact that αKlotho is phosphaturic, high Pi paradoxically but reproducibly induces αKlotho deficiency in mice (12, 40); with interesting disparity in normal humans (77). In addition, αKlotho deficiency decreases autophagic flux *in vivo* and *in vitro* (36). All of the above effects are associated with aging. The deleterious effect of high Pi and the beneficial effect of low Pi on aging and survival can be αKlotho-dependent or αKlotho-independent (10). Aging and high plasma Pi in *kl/kl* mice are ameliorated by restoration of αKlotho with viral delivery of αKlotho gene (78), transgenic overexpression αKlotho (32), or intraperitoneal administration of soluble αKlotho protein (79). Regardless of the congenital or acquired origin, the curent and previous published data (15, 36) suggest that αKlotho deficiency may be instrumental in lowering autophagic flux either directly or indirectly by causing phosphotoxicity. Reduction of plasma Pi effectively and sufficiently prolongs lifespan and rescues aging in αKlotho null mice (10, 35) strongly proving the concept that abnormal Pi metabolism is a trigger or/and accelerator to aging progression.

High phosphate suppresses autophagy flux

The effect of high Pi diet on autophagic flux is not universally consistent (80–83); probably dependent upon different target cells, levels of Pi, length of exposure, and other concomitant stressors. We examined autophagy markers in the kidney of mice treated with a short-period (2 weeks) of high Pi diet and confirmed lower autophagic flux without inducing hyperphosphatemia. Our cell culture experiments in OKP cells, a renal epithelial cell line (36, 84) offered direct and unequivocal evidence that high ambient Pi reduces autophagy flux; both LC3-I and LC3-II proteins were increased as well as elevation of p62, suggesting blockade of autophagic flux. Electron photomicrographs showed significantly fewer autophagosomes and autolysosomes, but massive accumulation of MLBs delimited by single

plasma membrane (56) in cells treated with high Pi media. The accumulated MLBs have been proposed to be related to deficiency of fusion of autophagosomes with lysosomes or/and lysosomal disorders (57, 58), which eventually disturbs autophagy flux (58, 85–87). It appears that there are potentially more than one mechanisms through which, high Pi reduces autophagy flux. High Pi decreases autophagosome formation through promoting beclin 1/BCL2 complex, and impairs autophagosome-lysosome function consequently blocking autophagosome and autolysosome recycling. However, high Pi-induced low autophagy in mice is likely a combined outcome of both direct Pi effects and indirect effects from αKlotho donwregulation.

Limitations—(1) Because no αKlotho knockout line was used in this study; we are not able to investigate whether beclin 1 prolongs mouse lifespan completely independently of αKlotho. Based on the time course of plasma Pi and αKlotho during *BK/BK;kl/kl* mice development, and the rapamycin effect on *kl/kl* mice, we proposed that beclin 1-induced phosphaturia decreases plasma Pi, consequently restoring αKlotho and rescuing prematuring age phenotypes. The beneficial effects of plasma Pi reduction after rapamycin administration (63), or through knockout of NaPi-2a on αKlotho knockout mice support direct Pi toxic effect on accelerating aging (10) that is αKlotho-independent. (2) Due to limited blood sample volumes, we did not measure PTH, another important mineral hormone participating in Pi homeostasis. So we could not exclude PTH's role in our *in vivo* models. (3) The current proof-of-conceptual study provides evidence to support that high Pi stabilizes and αKlotho disrupts beclin 1/BCL2 complex respectively. However, the mechanism(s) of modulation of the complex formation remain to be studied in the future. (4) High Pi-induced MLBs accumulation in cells is interesting but how high Pi induces aberrant contents degradation in autolysosomes needs to be explored.

In conclusion—Phosphate, autophagy, and αKlotho function as a closely interwoven tripartite network in health maintenance. Beclin 1 suppresses renal NaPi-2a/2c expression, increases phosphaturia, and reduces plasma Pi. Low plasma Pi upregulates αKlotho which further combats aging. High plasma Pi suppresses while αKlotho stimulates autophagy. Autophagy and αKlotho interactively counteract phosphotoxicity, prolong lifespan and attenuate aging-associated multiple organ degeneration (Fig. 1A).

Supplementary Material

Refer to Web version on PubMed Central for supplementary material.

ACKNOWLEDGMENTS

The authors would like to thank Dr. Noboru Mizushima (Tokyo Medical and Dental University, Tokyo, Japan) for providing the transgenic GFP-LC3 reporter mice and eGFP-LC3 plasmid. The authors are grateful to the expertise of Dr. Peng Li, Ms. Nancy Gillings and Mr. Jianning Zhang in the experiments and Dr. Vishal Patel for critical reading of this manuscript. This work was supported by NIH grants R01-CA109618 (B.L.), R01-DK091392 and R01-DK092461 (B.L., O.W.M., and M.C.H.), UT Southwestern Medical Center O'Brien Kidney Research Center (P30-DK07938) (O.W.M.), U19AI199725 (B.L.), a Fondation Leducq grant 15CBD04 (B.L., S.S., A.F.F.), the Simmons Family Foundation grant (O.W.M.), the Pak Center Innovative Research Support, Endowed Professors Collaborative Research Support, and the Pak-Seldin Center for Metabolic Research (O.W.M. and M.C.H.).

ABBREVIATIONS

ANOVA	analysis of variance
BCL2^{AAA}	BCL2AAA knock-in
Becn1$^{+/-}$	heterozygous global Becn1 knockout
BK	Becn1F121A knock-in
CVD	cardiovascular disease
CKD	chronic kidney disease
CQ	chloroquine
cDNA	complimentary DNA
ELISA	enzyme-linked immunosorbent assay
FGF23	fibroblast growth factor-23
GAPDH	glyceraldehyde-3-phosphate dehydrogenase
H&E	Hematoxylin and Eosin
***kl*/+**	heterozygous αKlotho hypomorphic
LDH	lactic acid dehydrogenase
LTL	Lotus Tetragonolobus lectin
MLB	multi-lamellar body
NaPi-2a	Na-dependent Pi cotransporter type II a
NaPi-2c	Na-dependent Pi cotransporter type II c
OKP	opossum kidney cell PTH responsive
Pi	inorganic phosphate
PTH	parathyroid hormone
Tg-kl	transgenic αKlotho overexpression
qPCR	quantitative polymerase chain reaction
SD	standard deviation
TC	trichrome
WGA	wheat germ agglutinin
WT	wild type

REFERENCES

1. AlGhatrif M, Wang M, Fedorova OV, Bagrov AY, and Lakatta EG (2017) The Pressure of Aging. Med Clin North Am 101, 81–101 [PubMed: 27884238]
2. Pletcher SD, and Stumpf MP (2002) Population genomics: ageing by association. Curr Biol 12, R328–330 [PubMed: 12007435]
3. Russell SJ, and Kahn CR (2007) Endocrine regulation of ageing. Nat Rev Mol Cell Biol 8, 681–691 [PubMed: 17684529]
4. Chang AR, Lazo M, Appel LJ, Gutierrez OM, and Grams ME (2014) High dietary phosphorus intake is associated with all-cause mortality: results from NHANES III. Am J Clin Nutr 99, 320–327 [PubMed: 24225358]
5. Ritter CS, and Slatopolsky E (2016) Phosphate Toxicity in CKD: The Killer among Us. Clin J Am Soc Nephrol 11, 1088–1100 [PubMed: 26912542]
6. Takeda E, Yamamoto H, Nashiki K, Sato T, Arai H, and Taketani Y (2004) Inorganic phosphate homeostasis and the role of dietary phosphorus. J Cell Mol Med 8, 191–200 [PubMed: 15256067]
7. Hu MC, Shiizaki K, Kuro-o M, and Moe OW (2013) Fibroblast growth factor 23 and Klotho: physiology and pathophysiology of an endocrine network of mineral metabolism. Annu Rev Physiol 75, 503–533 [PubMed: 23398153]
8. Kuro-o M (2010) A potential link between phosphate and aging--lessons from Klotho-deficient mice. Mech Ageing Dev 131, 270–275 [PubMed: 20197072]
9. McGovern AP, de Lusignan S, van Vlymen J, Liyanage H, Tomson CR, Gallagher H, Rafiq M, and Jones S (2013) Serum phosphate as a risk factor for cardiovascular events in people with and without chronic kidney disease: a large community based cohort study. PLoS One 8, e74996 [PubMed: 24040373]
10. Ohnishi M, and Razzaque MS (2010) Dietary and genetic evidence for phosphate toxicity accelerating mammalian aging. FASEB J 24, 3562–3571 [PubMed: 20418498]
11. Osuka S, and Razzaque MS (2012) Can features of phosphate toxicity appear in normophosphatemia? J Bone Miner Metab 30, 10–18 [PubMed: 22219005]
12. Hu MC, Shi M, Cho HJ, Adams-Huet B, Paek J, Hill K, Shelton J, Amaral AP, Faul C, Taniguchi M, Wolf M, Brand M, Takahashi M, Kuro OM, Hill JA, and Moe OW (2015) Klotho and phosphate are modulators of pathologic uremic cardiac remodeling. J Am Soc Nephrol 26, 1290–1302 [PubMed: 25326585]
13. Feng Y, He D, Yao Z, and Klionsky DJ (2014) The machinery of macroautophagy. Cell Res 24, 24–41 [PubMed: 24366339]
14. Hansen M, Rubinsztein DC, and Walker DW (2018) Autophagy as a promoter of longevity: insights from model organisms. Nat Rev Mol Cell Biol 19, 579–593 [PubMed: 30006559]
15. Fernandez AF, Sebti S, Wei Y, Zou Z, Shi M, McMillan KL, He C, Ting T, Liu Y, Chiang WC, Marciano DK, Schiattarella GG, Bhagat G, Moe OW, Hu MC, and Levine B (2018) Disruption of the beclin 1-BCL2 autophagy regulatory complex promotes longevity in mice. Nature 558, 136–140 [PubMed: 29849149]
16. Pyo JO, Yoo SM, Ahn HH, Nah J, Hong SH, Kam TI, Jung S, and Jung YK (2013) Overexpression of Atg5 in mice activates autophagy and extends lifespan. Nat Commun 4, 2300 [PubMed: 23939249]
17. Rocchi A, Yamamoto S, Ting T, Fan Y, Sadleir K, Wang Y, Zhang W, Huang S, Levine B, Vassar R, and He C (2017) A Becn1 mutation mediates hyperactive autophagic sequestration of amyloid oligomers and improved cognition in Alzheimer's disease. PLoS Genet 13, e1006962 [PubMed: 28806762]
18. Kuro-o M, Matsumura Y, Aizawa H, Kawaguchi H, Suga T, Utsugi T, Ohyama Y, Kurabayashi M, Kaname T, Kume E, Iwasaki H, Iida A, Shiraki-Iida T, Nishikawa S, Nagai R, and Nabeshima YI (1997) Mutation of the mouse klotho gene leads to a syndrome resembling ageing. Nature 390, 45–51 [PubMed: 9363890]
19. Kurosu H, Ogawa Y, Miyoshi M, Yamamoto M, Nandi A, Rosenblatt KP, Baum MG, Schiavi S, Hu MC, Moe OW, and Kuro-o M (2006) Regulation of fibroblast growth factor-23 signaling by klotho. J Biol Chem 281, 6120–6123 [PubMed: 16436388]

20. Kuro OM (2019) The Klotho proteins in health and disease. Nat Rev Nephrol 15, 27–44 [PubMed: 30455427]
21. Kuro-o M (2006) Klotho as a regulator of fibroblast growth factor signaling and phosphate/calcium metabolism. Curr Opin Nephrol Hypertens 15, 437–441 [PubMed: 16775459]
22. Urakawa I, Yamazaki Y, Shimada T, Iijima K, Hasegawa H, Okawa K, Fujita T, Fukumoto S, and Yamashita T (2006) Klotho converts canonical FGF receptor into a specific receptor for FGF23. Nature 444, 770–774 [PubMed: 17086194]
23. Goetz R, Nakada Y, Hu MC, Kurosu H, Wang L, Nakatani T, Shi M, Eliseenkova AV, Razzaque MS, Moe OW, Kuro-o M, and Mohammadi M (2010) Isolated C-terminal tail of FGF23 alleviates hypophosphatemia by inhibiting FGF23-FGFR-Klotho complex formation. Proc Natl Acad Sci U S A 107, 407–412 [PubMed: 19966287]
24. Hu MC, Shi M, Zhang J, Pastor J, Nakatani T, Lanske B, Razzaque MS, Rosenblatt KP, Baum MG, Kuro-o M, and Moe OW (2010) Klotho: a novel phosphaturic substance acting as an autocrine enzyme in the renal proximal tubule. FASEB J 24, 3438–3450 [PubMed: 20466874]
25. Consortium A (2000) Autosomal dominant hypophosphataemic rickets is associated with mutations in FGF23. Nat Genet 26, 345–348 [PubMed: 11062477]
26. Hu MC, Shi M, Zhang J, Addo T, Cho HJ, Barker SL, Ravikumar P, Gillings N, Bian A, Sidhu SS, Kuro-o M, and Moe OW (2016) Renal Production, Uptake, and Handling of Circulating alphaKlotho. J Am Soc Nephrol 27, 79–90 [PubMed: 25977312]
27. Chen CD, Podvin S, Gillespie E, Leeman SE, and Abraham CR (2007) Insulin stimulates the cleavage and release of the extracellular domain of Klotho by ADAM10 and ADAM17. Proc Natl Acad Sci U S A 104, 19796–19801 [PubMed: 18056631]
28. Bloch L, Sineshchekova O, Reichenbach D, Reiss K, Saftig P, Kuro-o M, and Kaether C (2009) Klotho is a substrate for alpha-, beta- and gamma-secretase. FEBS Lett 583, 3221–3224 [PubMed: 19737556]
29. Neyra JA, and Hu MC (2017) Potential application of klotho in human chronic kidney disease. Bone 100, 41–49 [PubMed: 28115282]
30. Lu X, and Hu MC (2017) Klotho/FGF23 Axis in Chronic Kidney Disease and Cardiovascular Disease. Kidney Dis (Basel) 3, 15–23 [PubMed: 28785560]
31. Chen G, Liu Y, Goetz R, Fu L, Jayaraman S, Hu MC, Moe OW, Liang G, Li X, and Mohammadi M (2018) alpha-Klotho is a non-enzymatic molecular scaffold for FGF23 hormone signalling. Nature 553, 461–466 [PubMed: 29342138]
32. Kurosu H, Yamamoto M, Clark JD, Pastor JV, Nandi A, Gurnani P, McGuinness OP, Chikuda H, Yamaguchi M, Kawaguchi H, Shimomura I, Takayama Y, Herz J, Kahn CR, Rosenblatt KP, and Kuro-o M (2005) Suppression of aging in mice by the hormone Klotho. Science 309, 1829–1833 [PubMed: 16123266]
33. Eren M, Boe AE, Murphy SB, Place AT, Nagpal V, Morales-Nebreda L, Urich D, Quaggin SE, Budinger GR, Mutlu GM, Miyata T, and Vaughan DE (2014) PAI-1-regulated extracellular proteolysis governs senescence and survival in Klotho mice. Proc Natl Acad Sci U S A 111, 7090–7095 [PubMed: 24778222]
34. Watanabe R, Fujita N, Sato Y, Kobayashi T, Morita M, Oike T, Miyamoto K, Kuro OM, Michigami T, Fukumoto S, Tsuji T, Toyama Y, Nakamura M, Matsumoto M, and Miyamoto T (2017) Enpp1 is an anti-aging factor that regulates Klotho under phosphate overload conditions. Sci Rep 7, 7786 [PubMed: 28798354]
35. Ohnishi M, Nakatani T, Lanske B, and Razzaque MS (2009) In vivo genetic evidence for suppressing vascular and soft-tissue calcification through the reduction of serum phosphate levels, even in the presence of high serum calcium and 1,25-dihydroxyvitamin d levels. Circ Cardiovasc Genet 2, 583–590 [PubMed: 20031638]
36. Shi M, Flores B, Gillings N, Bian A, Cho HJ, Yan S, Liu Y, Levine B, Moe OW, and Hu MC (2016) alphaKlotho Mitigates Progression of AKI to CKD through Activation of Autophagy. J Am Soc Nephrol 27, 2331–2345 [PubMed: 26701976]
37. Qu X, Yu J, Bhagat G, Furuya N, Hibshoosh H, Troxel A, Rosen J, Eskelinen EL, Mizushima N, Ohsumi Y, Cattoretti G, and Levine B (2003) Promotion of tumorigenesis by heterozygous disruption of the beclin 1 autophagy gene. J Clin Invest 112, 1809–1820 [PubMed: 14638851]

38. He C, Bassik MC, Moresi V, Sun K, Wei Y, Zou Z, An Z, Loh J, Fisher J, Sun Q, Korsmeyer S, Packer M, May HI, Hill JA, Virgin HW, Gilpin C, Xiao G, Bassel-Duby R, Scherer PE, and Levine B (2012) Exercise-induced BCL2-regulated autophagy is required for muscle glucose homeostasis. Nature 481, 511–515 [PubMed: 22258505]
39. Hu MC, Shi M, Zhang J, Quinones H, Kuro-o M, and Moe OW (2010) Klotho deficiency is an early biomarker of renal ischemia-reperfusion injury and its replacement is protective. Kidney Int 78, 1240–1251 [PubMed: 20861825]
40. Hu MC, Shi M, Gillings N, Flores B, Takahashi M, Kuro OM, and Moe OW (2017) Recombinant alpha-Klotho may be prophylactic and therapeutic for acute to chronic kidney disease progression and uremic cardiomyopathy. Kidney Int 91, 1104–1114 [PubMed: 28131398]
41. Bian A, Shi M, Flores B, Gillings N, Li P, Yan SX, Levine B, Xing C, and Hu MC (2017) Downregulation of autophagy is associated with severe ischemia-reperfusion-induced acute kidney injury in overexpressing C-reactive protein mice. PLoS One 12, e0181848 [PubMed: 28886014]
42. Vega-Rubin-de-Celis S, Zou Z, Fernandez AF, Ci B, Kim M, Xiao G, Xie Y, and Levine B (2018) Increased autophagy blocks HER2-mediated breast tumorigenesis. Proc Natl Acad Sci U S A 115, 4176–4181 [PubMed: 29610308]
43. Peraro L, Zou Z, Makwana KM, Cummings AE, Ball HL, Yu H, Lin YS, Levine B, and Kritzer JA (2017) Diversity-Oriented Stapling Yields Intrinsically Cell-Penetrant Inducers of Autophagy. J Am Chem Soc 139, 7792–7802 [PubMed: 28414223]
44. Barker SL, Pastor J, Carranza D, Quinones H, Griffith C, Goetz R, Mohammadi M, Ye J, Zhang J, Hu MC, Kuro-o M, Moe OW, and Sidhu SS (2015) The demonstration of alphaKlotho deficiency in human chronic kidney disease with a novel synthetic antibody. Nephrol Dial Transplant 30, 223–233 [PubMed: 25324355]
45. Hu MC, Shi M, Zhang J, Quinones H, Griffith C, Kuro-o M, and Moe OW (2011) Klotho deficiency causes vascular calcification in chronic kidney disease. J Am Soc Nephrol 22, 124–136 [PubMed: 21115613]
46. Liu Y, Shoji-Kawata S, Sumpter RM Jr., Wei Y, Ginet V, Zhang L, Posner B, Tran KA, Green DR, Xavier RJ, Shaw SY, Clarke PG, Puyal J, and Levine B (2013) Autosis is a Na+,K+-ATPase-regulated form of cell death triggered by autophagy-inducing peptides, starvation, and hypoxia-ischemia. Proc Natl Acad Sci U S A 110, 20364–20371 [PubMed: 24277826]
47. Shi M, Flores B, Li P, Gillings N, McMillan KL, Ye J, Huang LJ, Sidhu SS, Zhong YP, Grompe MT, Streeter PR, Moe OW, and Hu MC (2017) Effects of Erythropoietin Receptor Activity on Angiogenesis, Tubular Injury and Fibrosis in Acute Kidney Injury: A “U-Shaped” Relationship. Am J Physiol Renal Physiol, ajprenal 00306 02017
48. Faul C, Amaral AP, Oskouei B, Hu MC, Sloan A, Isakova T, Gutierrez OM, Aguillon-Prada R, Lincoln J, Hare JM, Mundel P, Morales A, Scialla J, Fischer M, Soliman EZ, Chen J, Go AS, Rosas SE, Nessel L, Townsend RR, Feldman HI, St John Sutton M, Ojo A, Gadegbeku C, Di Marco GS, Reuter S, Kentrup D, Tiemann K, Brand M, Hill JA, Moe OW, Kuro OM, Kusek JW, Keane MG, and Wolf M (2011) FGF23 induces left ventricular hypertrophy. J Clin Invest 121, 4393–4408 [PubMed: 21985788]
49. Shi M, McMillan KL, Wu J, Gillings N, Flores B, Moe OW, and Hu MC (2018) Cisplatin nephrotoxicity as a model of chronic kidney disease. Lab Invest 98, 1105–1121 [PubMed: 29858580]
50. Biber J, Hernando N, Forster I, and Murer H (2009) Regulation of phosphate transport in proximal tubules. Pflugers Arch 458, 39–52 [PubMed: 18758808]
51. Yue Z, Jin S, Yang C, Levine AJ, and Heintz N (2003) Beclin 1, an autophagy gene essential for early embryonic development, is a haploinsufficient tumor suppressor. Proc Natl Acad Sci U S A 100, 15077–15082 [PubMed: 14657337]
52. Hu MC, Kuro-o M, and Moe OW (2014) alphaKlotho and vascular calcification: an evolving paradigm. Curr Opin Nephrol Hypertens 23, 331–339 [PubMed: 24867676]
53. Takeshita K, Fujimori T, Kurotaki Y, Honjo H, Tsujikawa H, Yasui K, Lee JK, Kamiya K, Kitaichi K, Yamamoto K, Ito M, Kondo T, Iino S, Inden Y, Hirai M, Murohara T, Kodama I, and Nabeshima Y (2004) Sinoatrial node dysfunction and early unexpected death of mice with a defect of klotho gene expression. Circulation 109, 1776–1782 [PubMed: 15037532]

54. Gansevoort RT, Correa-Rotter R, Hemmelgarn BR, Jafar TH, Heerspink HJ, Mann JF, Matsushita K, and Wen CP (2013) Chronic kidney disease and cardiovascular risk: epidemiology, mechanisms, and prevention. Lancet 382, 339–352 [PubMed: 23727170]

55. Crawford NM, and Steiner AZ (2015) Age-related infertility. Obstet Gynecol Clin North Am 42, 15–25 [PubMed: 25681837]

56. Schmitz G, and Muller G (1991) Structure and function of lamellar bodies, lipid-protein complexes involved in storage and secretion of cellular lipids. J Lipid Res 32, 1539–1570 [PubMed: 1797938]

57. Hariri M, Millane G, Guimond MP, Guay G, Dennis JW, and Nabi IR (2000) Biogenesis of multilamellar bodies via autophagy. Mol Biol Cell 11, 255–268 [PubMed: 10637306]

58. Garcia-Sanz P, Orgaz L, Fuentes JM, Vicario C, and Moratalla R (2018) Cholesterol and multilamellar bodies: Lysosomal dysfunction in GBA-Parkinson disease. Autophagy 14, 717–718 [PubMed: 29368986]

59. Shoji-Kawata S, Sumpter R, Leveno M, Campbell GR, Zou Z, Kinch L, Wilkins AD, Sun Q, Pallauf K, MacDuff D, Huerta C, Virgin HW, Helms JB, Eerland R, Tooze SA, Xavier R, Lenschow DJ, Yamamoto A, King D, Lichtarge O, Grishin NV, Spector SA, Kaloyanova DV, and Levine B (2013) Identification of a candidate therapeutic autophagy-inducing peptide. Nature 494, 201–206 [PubMed: 23364696]

60. Scialla JJ, and Wolf M (2014) Roles of phosphate and fibroblast growth factor 23 in cardiovascular disease. Nat Rev Nephrol 10, 268–278 [PubMed: 24686452]

61. Morishita K, Shirai A, Kubota M, Katakura Y, Nabeshima Y, Takeshige K, and Kamiya T (2001) The progression of aging in klotho mutant mice can be modified by dietary phosphorus and zinc. J Nutr 131, 3182–3188 [PubMed: 11739863]

62. Schwarz C, Bohmig GA, Steininger R, Mayer G, and Oberbauer R (2001) Impaired phosphate handling of renal allografts is aggravated under rapamycin-based immunosuppression. Nephrol Dial Transplant 16, 378–382 [PubMed: 11158416]

63. Kawai M, Kinoshita S, Ozono K, and Michigami T (2016) Inorganic Phosphate Activates the AKT/mTORC1 Pathway and Shortens the Life Span of an alphaKlotho-Deficient Model. J Am Soc Nephrol 27, 2810–2824 [PubMed: 26872488]

64. Kempe DS, Dermaku-Sopjani M, Frohlich H, Sopjani M, Umbach A, Puchchakayala G, Capasso A, Weiss F, Stubs M, Foller M, and Lang F (2010) Rapamycin-induced phosphaturia. Nephrol Dial Transplant 25, 2938–2944 [PubMed: 20368307]

65. Haller M, Amatschek S, Wilflingseder J, Kainz A, Bielesz B, Pavik I, Serra A, Mohebbi N, Biber J, Wagner CA, and Oberbauer R (2012) Sirolimus induced phosphaturia is not caused by inhibition of renal apical sodium phosphate cotransporters. PLoS One 7, e39229 [PubMed: 22859939]

66. Hoorn EJ, and Severs D (2017) Autophagy and renal epithelial transport: eat to survive. Kidney Int 91, 1003–1005 [PubMed: 28407874]

67. Lanning NJ, VanOpstall C, Goodall ML, MacKeigan JP, and Looyenga BD (2018) LRRK2 deficiency impairs trans-Golgi to lysosome trafficking and endocytic cargo degradation in human renal proximal tubule epithelial cells. Am J Physiol Renal Physiol 315, F1465–F1477 [PubMed: 30089035]

68. Khositseth S, Charngkaew K, Boonkrai C, Somparn P, Uawithya P, Chomanee N, Payne DM, Fenton RA, and Pisitkun T (2017) Hypercalcemia induces targeted autophagic degradation of aquaporin-2 at the onset of nephrogenic diabetes insipidus. Kidney Int 91, 1070–1087 [PubMed: 28139295]

69. Khositseth S, Uawithya P, Somparn P, Charngkaew K, Thippamom N, Hoffert JD, Saeed F, Michael Payne D, Chen SH, Fenton RA, and Pisitkun T (2015) Autophagic degradation of aquaporin-2 is an early event in hypokalemia-induced nephrogenic diabetes insipidus. Sci Rep 5, 18311 [PubMed: 26674602]

70. Wei W, An XR, Jin SJ, Li XX, and Xu M (2018) Inhibition of insulin resistance by PGE1 via autophagy-dependent FGF21 pathway in diabetic nephropathy. Sci Rep 8, 9 [PubMed: 29311680]

71. Cherqui S, and Courtoy PJ (2017) The renal Fanconi syndrome in cystinosis: pathogenic insights and therapeutic perspectives. Nat Rev Nephrol 13, 115–131 [PubMed: 27990015]

72. Grieco G, Janssens V, Gaide Chevronnay HP, N'Kuli F, Van Der Smissen P, Wang T, Shan J, Vainio S, Bilanges B, Jouret F, Vanhaesebroeck B, Pierreux CE, and Courtoy PJ (2018) Vps34/

PI3KC3 deletion in kidney proximal tubules impairs apical trafficking and blocks autophagic flux, causing a Fanconi-like syndrome and renal insufficiency. Sci Rep 8, 14133 [PubMed: 30237523]

73. Wagner CA, Rubio-Aliaga I, and Hernando N (2019) Renal phosphate handling and inherited disorders of phosphate reabsorption: an update. Pediatr Nephrol 34, 549–559 [PubMed: 29275531]
74. Biber J, Hernando N, and Forster I (2013) Phosphate transporters and their function. Annu Rev Physiol 75, 535–550 [PubMed: 23398154]
75. Hu MC, Shi M, and Moe OW (2019) Role of alphaKlotho and FGF23 in regulation of type II Na-dependent phosphate co-transporters. Pflugers Arch 471, 99–108 [PubMed: 30506274]
76. Bian A, Xing C, and Hu MC (2014) Alpha Klotho and phosphate homeostasis. J Endocrinol Invest 37, 1121–1126 [PubMed: 25194425]
77. Scanni R, vonRotz M, Jehle S, Hulter HN, and Krapf R (2014) The human response to acute enteral and parenteral phosphate loads. J Am Soc Nephrol 25, 2730–2739 [PubMed: 24854273]
78. Shiraki-Iida T, Iida A, Nabeshima Y, Anazawa H, Nishikawa S, Noda M, Kuro-o M, and Nabeshima Y (2000) Improvement of multiple pathophysiological phenotypes of klotho (kl/kl) mice by adenovirus-mediated expression of the klotho gene. J Gene Med 2, 233–242 [PubMed: 10953914]
79. Chen TH, Kuro OM, Chen CH, Sue YM, Chen YC, Wu HH, and Cheng CY (2013) The secreted Klotho protein restores phosphate retention and suppresses accelerated aging in Klotho mutant mice. Eur J Pharmacol 698, 67–73 [PubMed: 23041151]
80. Dai XY, Zhao MM, Cai Y, Guan QC, Zhao Y, Guan Y, Kong W, Zhu WG, Xu MJ, and Wang X (2013) Phosphate-induced autophagy counteracts vascular calcification by reducing matrix vesicle release. Kidney Int 83, 1042–1051 [PubMed: 23364520]
81. Zhang YY, Yang M, Bao JF, Gu LJ, Yu HL, and Yuan WJ (2018) Phosphate stimulates myotube atrophy through autophagy activation: evidence of hyperphosphatemia contributing to skeletal muscle wasting in chronic kidney disease. BMC Nephrol 19, 45 [PubMed: 29486729]
82. Shanahan CM (2013) Autophagy and matrix vesicles: new partners in vascular calcification. Kidney Int 83, 984–986 [PubMed: 23727998]
83. Hsu YJ, Hsu SC, Huang SM, Lee HS, Lin SH, Tsai CS, Shih CC, and Lin CY (2015) Hyperphosphatemia induces protective autophagy in endothelial cells through the inhibition of Akt/mTOR signaling. J Vasc Surg 62, 210–221 e212 [PubMed: 24797554]
84. Hu MC, Fan L, Crowder LA, Karim-Jimenez Z, Murer H, and Moe OW (2001) Dopamine acutely stimulates Na+/H+ exchanger (NHE3) endocytosis via clathrin-coated vesicles: dependence on protein kinase A-mediated NHE3 phosphorylation. J Biol Chem 276, 26906–26915 [PubMed: 11328806]
85. Pous C, and Codogno P (2011) Lysosome positioning coordinates mTORC1 activity and autophagy. Nat Cell Biol 13, 342–344 [PubMed: 21460804]
86. Dunn WA Jr. (1994) Autophagy and related mechanisms of lysosome-mediated protein degradation. Trends Cell Biol 4, 139–143 [PubMed: 14731737]
87. Zhang X, Yu L, and Xu H (2016) Lysosome calcium in ROS regulation of autophagy. Autophagy 12, 1954–1955 [PubMed: 27485905]

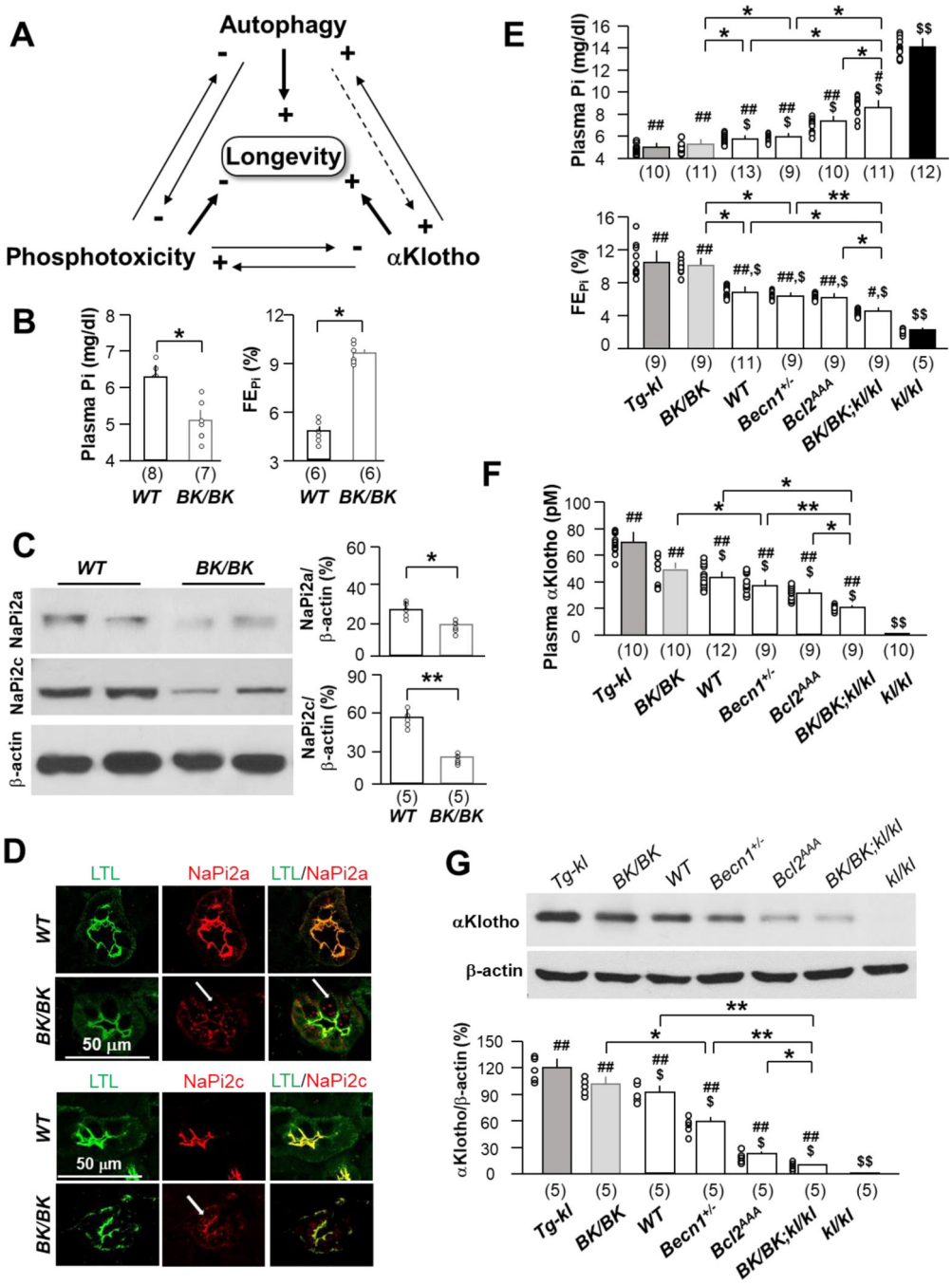

Fig. 1. High autophagic flux-induced improvement of phosphate homeostasis is associated with increased urinary phosphate excretion and αKlotho in the kidney and the circulation.

(**A**) Proposed model for interplay of Pi, autophagy, and αKlotho in health maintenance and prolongation of murine lifespan. Both autophagy and αKlotho suppress phosphotoxicity. High Pi inhibits both autophagy and αKlotho function. αKlotho also directly upregulates autophagy through reduction of the beclin 1/BCL2 complex, and autophagy upregulates αKlotho partly through reducing plasma Pi. Potentially high autophagy can directly stimulate αKlotho (dash line). Overall autophagy and αKlotho promote and high Pi reduces

longevity. (**B**) Plasma Pi (left panel) and fractional excretion of phosphate (FE_{Pi}) (right panel) of *WT* and *BK/BK* mice at 12 weeks-old without intervention. The data are presented at mean ± S.D. plus scatter plots of individual data points. (**C**) Immunoblots for NaPi-2a and −2c protein in the kidney of *WT* and *BK/BK* mice at 12 weeks-old. Left panel shows representative immunoblots. Right panel is quantitation of all blots from 5 mice in each group. Data are presented as mean ± S.D. *P<0.05, **P<0.01 between two groups by unpaired *t*-test for B - C. (**D**) Representative immunohistochemistry for NaPi-2a (upper two panel) and NaPi-2c (bottom two panel) in the kidney of *WT* and *BK/BK* mice at 12 weeks-old. Each genotype has 4 mice. Scale bar = 50 μm. Arrows indicate endocytosed NaPi-2a/2c. (**E**) Plasma phosphate (Pi) (upper panel) and fractional excretion of phosphate (FE_{Pi}) (bottom panel) and (**F**) plasma renal αKlotho in mice with different levels of αKlotho (*Tg-kl, WT,* and *kl/kl*) and different levels of autophagy flux (*BK/BK, Becn1*$^{+/-}$, *Bcl2*^{AAA}, *WT* and *BK/BK;kl/kl)* at 10 weeks-old. (**G**) renal αKlotho protein expression in mice with different levels of αKlotho (*Tg-kl, WT,* and *kl/kl*) and different levels of autophagy flux (*BK/BK, Becn1*$^{+/-}$, *Bcl2*^{AAA}, *WT* and *BK/BK;kl/kl)* at 10 weeks-old. Upper panel is representative blot for αKlotho protein; bottom panel is quantitation of all blots from 5 mice in each group. Data shown in **B**, **C**, and **E - G** are mean ± S.D. plus scatter plots of individual data points. *P<0.05, **P<0.01 between two groups; $^{\$}$P<0.05, $^{\$\,\$}$P<0.01 vs *Tg-kl* mice; $^{\#}$P<0.05, $^{\#\#}$P<0.01 vs *kl/kl* mice by one-way ANOVA followed by Student-Newman-Keuls *post hoc* test. The sample size of each genotype is shown in parentheses for **B**, **C**, and **E - G**.

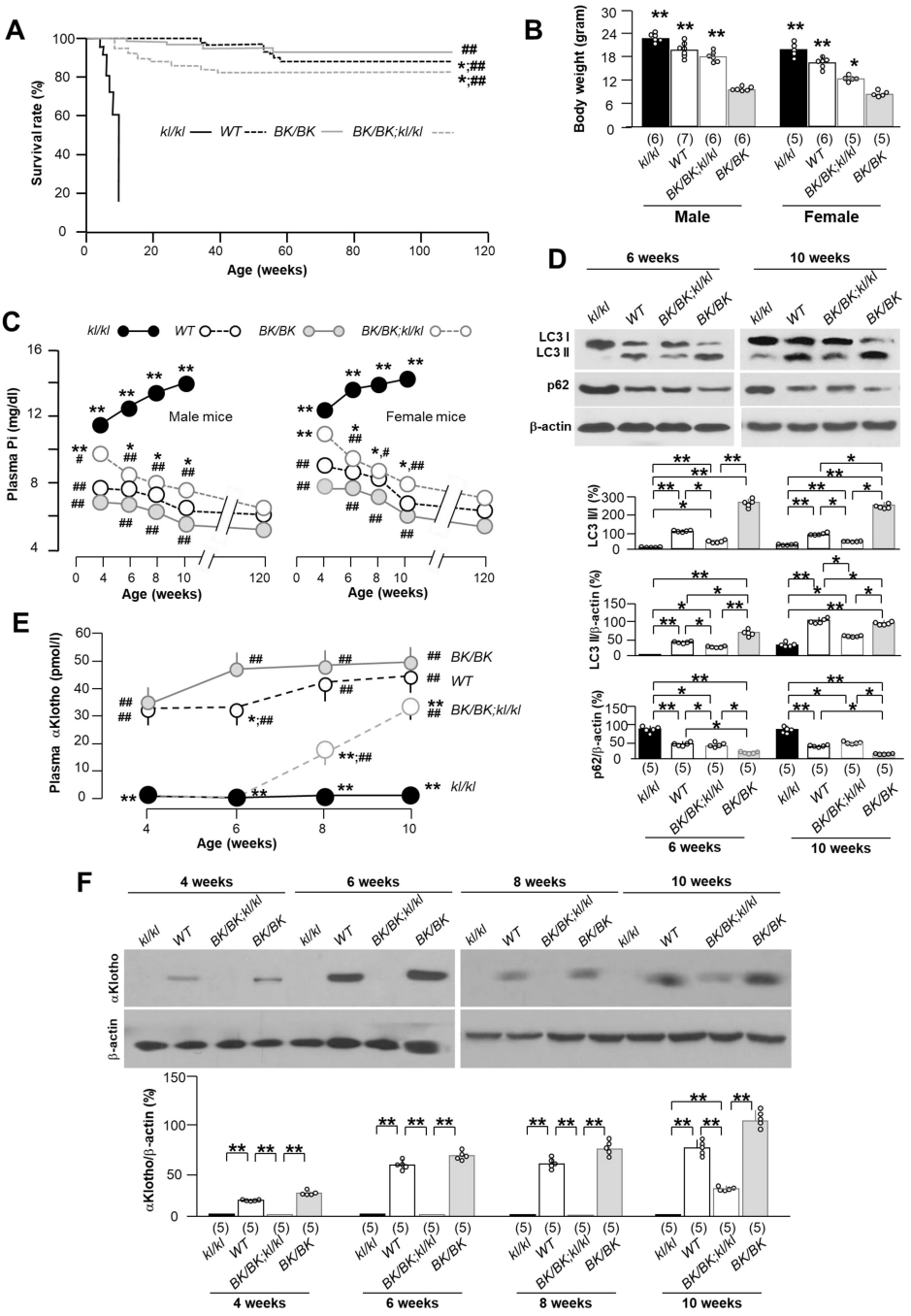

Fig. 2. Becn1F121A rescues premature aging, corrects hyperphosphatemia, circulating αKlotho levels, and restores autophagy activity and αKlotho in the kidney of *kl/kl* mice.

(**A**) Kaplan-Meier survival curves of different genotyping mice. *WT* (n=52), *Bk/BK* (n=61), *BK/BK;kl/kl* (n=63), and *kl/kl* (n=43) mice. *P<0.05 vs *BK/BK*, ##P<0.01 vs *kl/kl* mice by log-rank (Mantel-Cox) test. (**B**) Comparison of body weight of *WT*, *Bk/BK*, *BK/BK;kl/kl,* and *kl/kl* genotypes between male and female mice at the age of 10 weeks. The sample size of each genotype is shown in parentheses. Data are presented as mean ± S.D. with scatter plots of individual data points. **P<0.01 vs *kl/kl* mice by one-way ANOVA followed by

Student-Newman-Keuls *post hoc* test. (**C**) Change in plasma phosphate (Pi) in *WT* (n=46 in total including: male 23; female: 23); *Bk/BK* (n=40 in total including male: 20; female: 20); *BK/BK;kl/kl* (n=38 in total including male: 18; female 20); and *kl/kl* mice (n=28 in total including male: 13; female: 15). *P<0.05, **P<0.01 vs *BK/BK* mice, #P<0.05, ##P< 0.01 *kl/kl* mice groups by one-way ANOVA followed by Student-Newman-Keuls *post hoc* test at the indicated time point. **(D)** Immunoblots of total kidney lysates for LC3 and p62 protein in the kidneys of 4 genotypes at the age of 6 and 10 weeks, respectively. Upper panel shows representative immunoblots. Bottom panel summarizes data presented as mean ± S.D. Each group has 5 mice at each time point. *P<0.05, **P<0.01 between two groups by one-way ANOVA followed by Student-Newman-Keuls *post hoc* test. (**E**) Change in plasma αKlotho in *WT*; *Bk/BK*; *BK/BK;kl/kl*; and *kl/kl* mice at the age of 4, 6, 8 and 10 weeks respectively. The data were presented as mean ± S.D. with scatter plots of individual data points. Each genotype has 5 mice at each time point. *P<0.05 vs *BK/BK* and ##P<0.01 vs *kl/kl* by one-way ANOVA followed by Student-Newman-Keuls *post hoc* test at 10 weeks-old. (**F**) Renal αKlotho expression. Upper panel shows representative immunoblots of total kidney lysates for αKlotho protein in the kidney of 4 genotypes (*kl/kl*, *WT*, *BK/BK;kl/kl,* and *BK/BK* mice) at the age of 4, 6, 8 and 10 weeks respectively. Each genotype has 5 mice at each time point. Bottom panel is a summary of all blots and presented as mean ± S.D. with scatter plots of individual data points. *P<0.05, **P<0.01 between 2 groups at same time point by one-way ANOVA followed by Student-Newman-Keuls *post hoc* test.

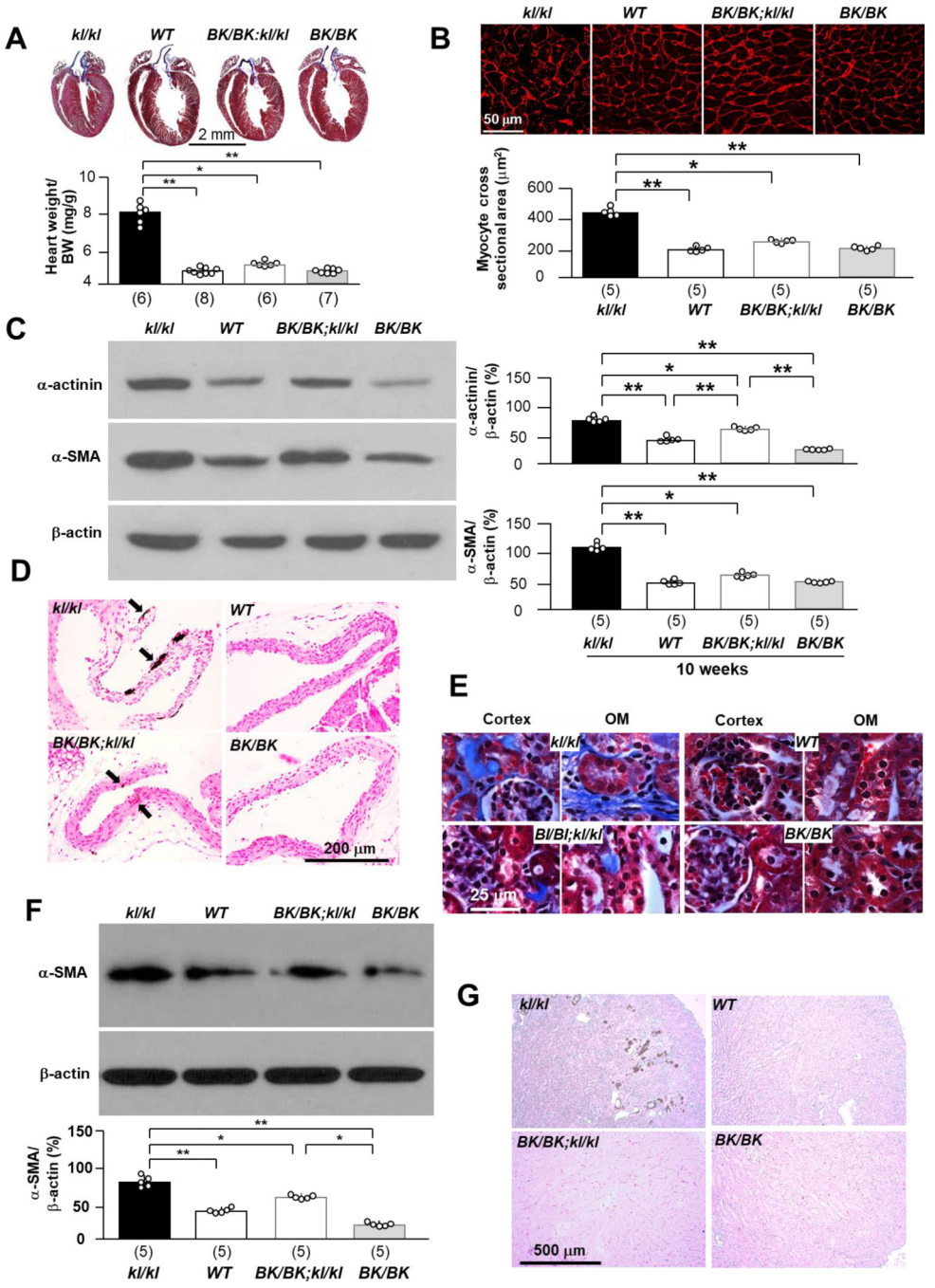

Fig. 3. Becn1^{F121A} rescues cardiac and renal phenotypes in *kl/kl* mice.

(**A**) Cardiac phenotypes in 4 genotypes (*kl/kl*, *WT*, *BK/BK;kl/kl,* and *BK/BK* mice) at the age of 10 weeks. Representative macrographs of heart sections stained with Trichrome. Bottom panel is summary data of heart weight over body weight. Scale bar = 2 mm. Number of mice of each genotype is shown in parenthesis at the bottom. (**B**) Representative microscopic images of WGA stained left ventricle sections of 5 mice from each genotype. Bottom panel is summary data. with scatter plots of individual data points. Scale bar = 50 μm. (**C**) Representative immunoblots of total left ventricular lysates for α-actinin and α-

SMA αKlotho protein in the heart of 5 mice from each genotype. Right panel is a summary of all immunoblots. (**D**) Vascular calcification in 4 genotypes at 10 weeks old. Representative microscopic images of Von Kossa stain in the aortic roots of 4 mice from each genotype. Scale bar = 200 μm. (**E**) Trichrome stain in the kidney sections of 4 genotypes at the age of 10 weeks. Representative microscopic images of Trichrome stain in the kidney sections of 6 mice from each genotype at 10 weeks. Scale bar = 25 μm. (**F**) Fibrotic marker, α-SMA protein expression in the kidneys. Upper panel shows representative immunoblots of total kidney lysates for α-SMA protein expression. Bottom panel is summary of data from 5 mice for each genotype. (**G**) Representative microscopic images of ectopic calcification in Von Kossa stained kidney sections from 4 mice for each genotype. Scale bar = 500 μm. Data shown in **A** - **C**, and **F** are means ± S.D. with scatter plots of individual data points. *P<0.05, **P<0.01 between two groups by one-way ANOVA followed by Student-Newman-Keuls *post hoc* test for **A** - **C**, and **F**.

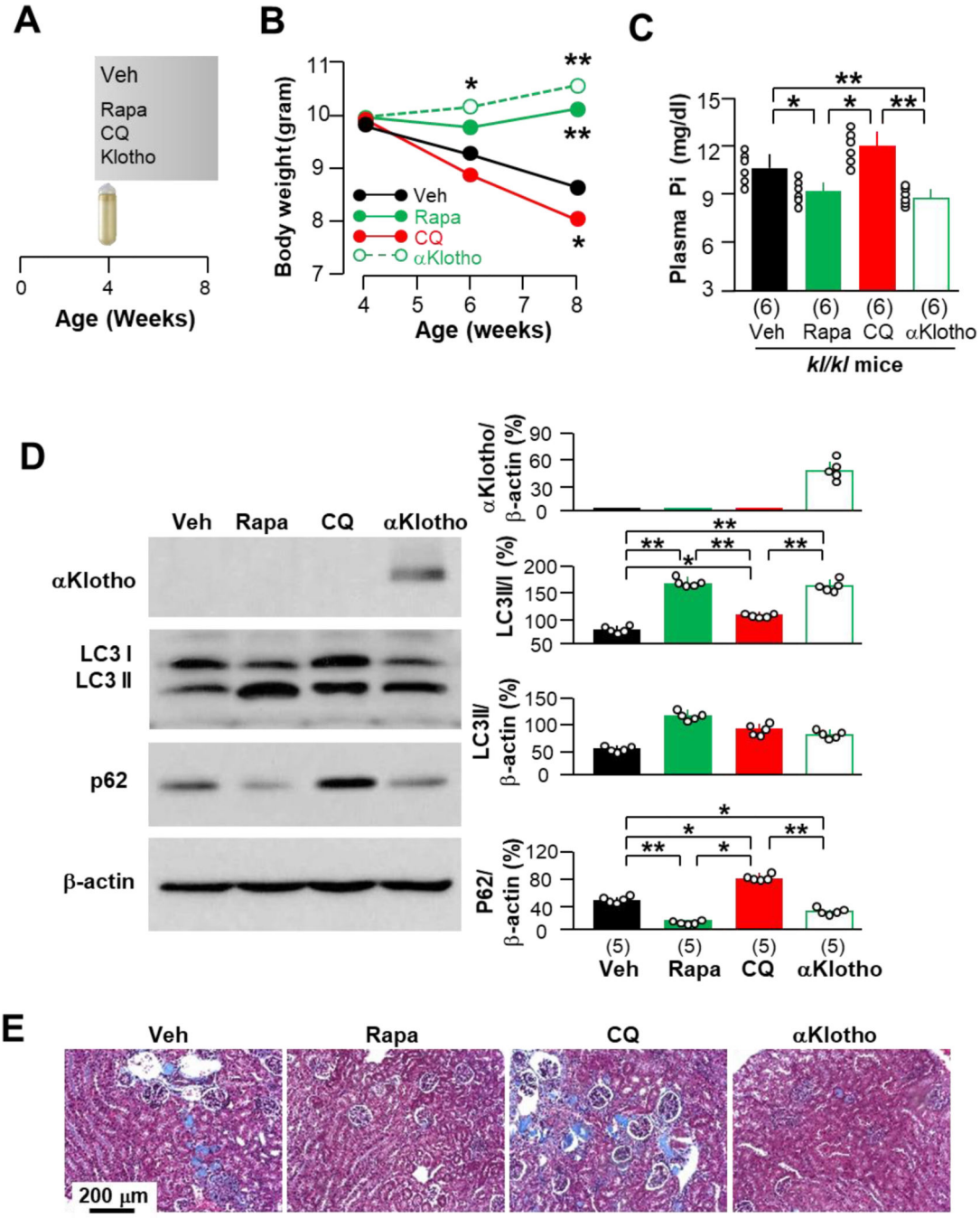

Fig. 4. Early effect of autophagy on Pi homeostasis and mouse growth is independent of αKlotho expression in *kl/kl* mice.

(**A**) Experimental design. *kl/kl* mice at 4 weeks were intraperitoneally given rapamycin (Rapa), chloroquine (CQ), recombinant αKlotho protein (αKlotho) or vehicle (normal saline) through osmotic minipumps. Four weeks after intraperitoneal administration, mice were sacrificed for **B** - **E**. Each group had 6 mice with equal male vs female number. (**B**) Body weight is presented as means from 6 mice per group. *P<0.05; **P<0.01 vs vehicle group between two groups by one-way ANOVA followed by Student-Newman-Keuls *post*

hoc test at indicated time point. (**C**) Plasma Pi of mice. Data are presented as means ± S.D. with scatter plots of individual data points for 6 mice per group. (**D**) Representative immunoblots of total kidney lysates for αKlotho, LC3 and p62 protein expression in the kidneys of 5 mice from each group. Right panel is summary of data from all blots. Data are presented as means ± S.D. with scatter plots of individual data points for 5 mice per group. *P<0.05, **P<0.01 between two groups by one-way ANOVA followed by Student-Newman-Keuls *post hoc* test for **C** and **D**. (**E**) Representative microscopic images of Trichrome stained kidney sections from 6 mice randomly selected from each group. Scale bar = 200 μm.

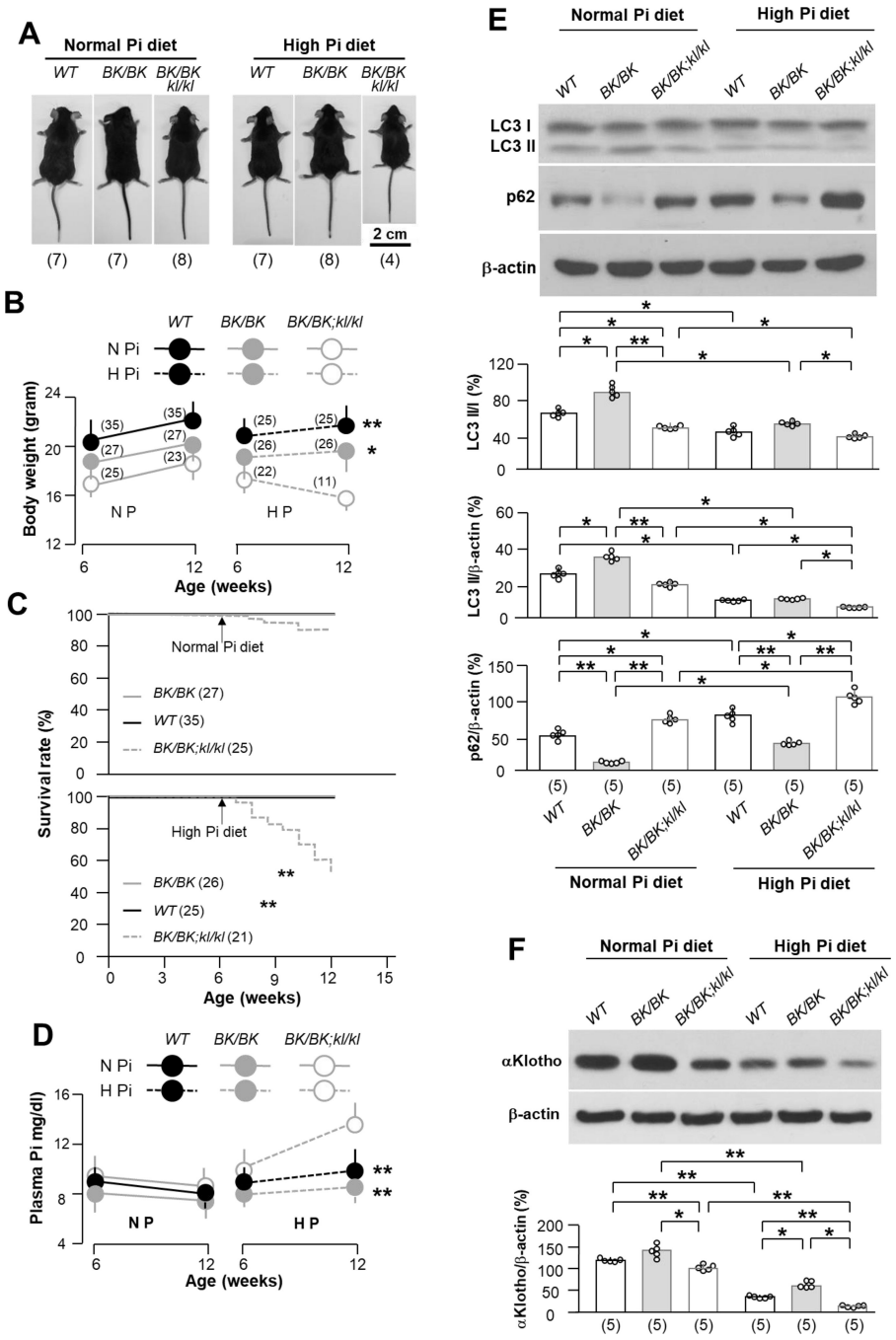

Fig. 5. High dietary Pi abolishes beneficial effect of becn1^{F121A} on prolonging life, growing, Pi metabolism and αKlotho upregulation in *kl/kl* mice.

(**A**) Comparison of mouse body size among 3 genotypes (*WT, BK/BK,* and *BK/BK;kl/kl*) treated normal (0.7%) or high (2.0%) Pi diet at 12 weeks old after 6-week treatment starting at 6 weeks old. Representative photos of male mouse bodies randomly selected from three genotypes. The animal number per treatment is shown in parenthesis at the bottom of photos. (**B**) Body weights of male and female mice of three genotypes at the beginning and the end of 6-week normal or high Pi treatment. The mouse number is shown in parenthesis.

Data are presented as means ± S.D. *P<0.05; **P<0.01 vs *BK/BK;kl/kl* mice after 6-week normal or high Pi diet by one-way ANOVA followed by Student-Newman-Keuls *post hoc* test. (**C**) Kaplan-Meier survival rate of three genotypes from 6 to 12 weeks during 6-weeks of normal or high dietary Pi. The animal number in each group is shown in parenthesis. ** P<0.01 *BK/BK;kl/kl* mice was determined by log-rank (Mantel-Cox) test. (**D**) Plasma Pi in 3 genotypes before and after normal or high Pi dietary treatment. Data are presented as means ± S.D. The animal number of each group is same as shown in Figure 5B. **P<0.01 vs *WT* mice after 6-week normal or high Pi diet by one-way ANOVA followed by Student-Newman-Keuls *post hoc* test at indicated time point. (**E**) Immunoblots of total kidney lysates for autophagic markers in the kidney of 3 genotypes treated with normal or high Pi diet. Upper panel shows representative blots from each treatment. Bottom panel is summary of data presented as mean ± S.D. with scatter plots of individual data points. Each group has 5 mice. (**F**) Immunoblots of total kidney lysates for αKlotho expression. Upper panel is representative blots from 5 mice for each treatment. Bottom panel is summarized data from all of blots presented as mean ± S.D. with scatter plots of individual data points. *P<0.05, **P<0.01 between two groups by two-way ANOVA followed by Student-Newman-Keuls *post hoc* test for **E** and **F**.

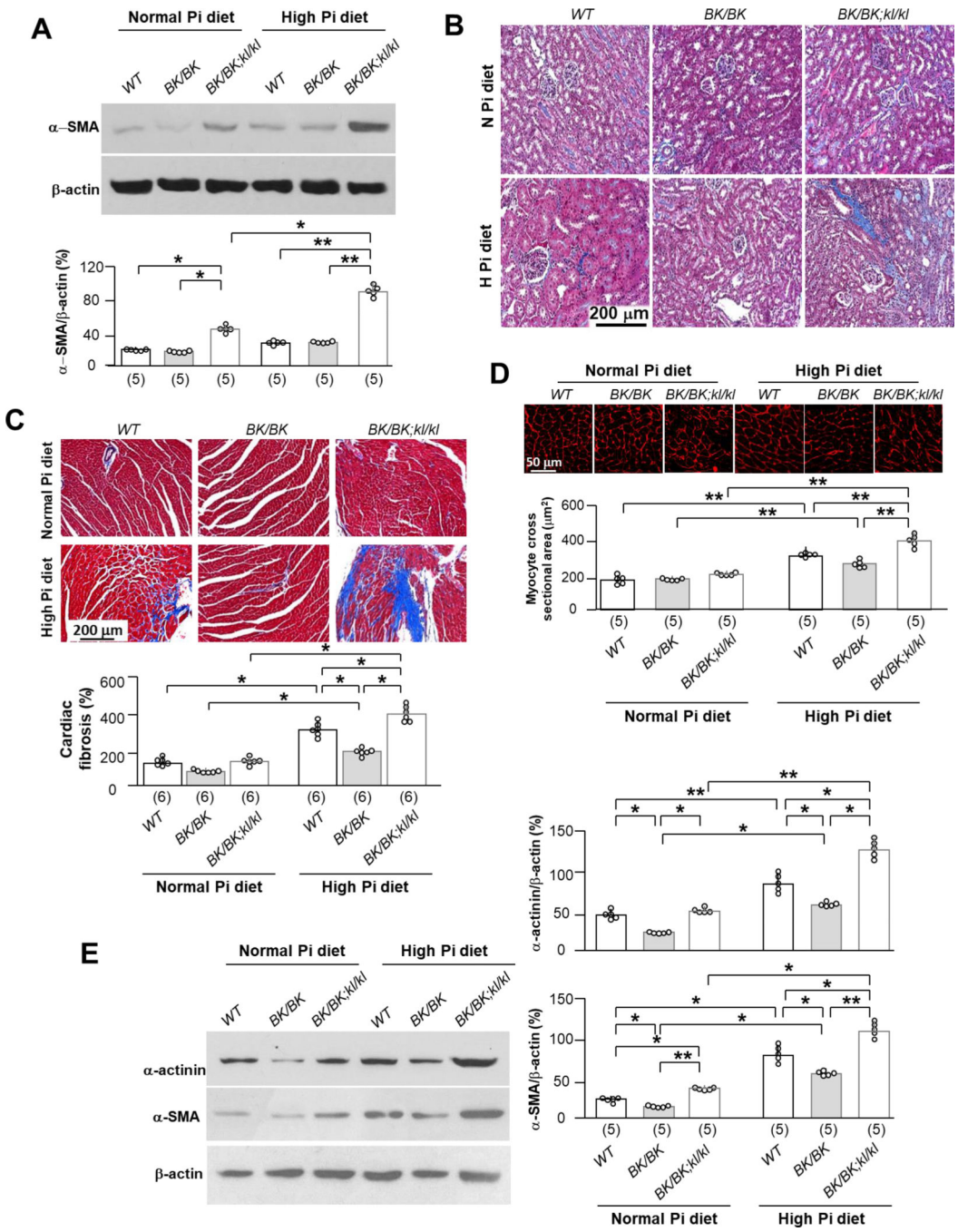

Fig. 6. High dietary Pi blocks beneficial renal and cardiac effect of becn1FA on *kl/kl* mice.

Mice of three genotypes (*WT, BK/BK,* and *BK/BK;kl/kl*) were treated with normal or high Pi diet for 6 weeks starting at 6 weeks old as mentioned in Figure 4. (**A**) Immunoblots of total kidney lysates for α-SMA expression. Upper panel is representative blots from each treatment. Bottom panel is summarized data presented as mean ± S.D. with scatter plots of individual data points. Each treatment has 5 mice. (**B**) Trichrome stain in the kidney sections of 3 genotypes after 6-week dietary Pi treatment. Representative microscopic images of Trichrome stain in kidney sections from each treatment. Scale bar = 200 μm. Each treatment

has 5 mice. (**C**) Representative microscopic images of Trichrome stained heart sections. Each genotype has 6 mice. Scale bar = 200 μm. Bottom panel summarizes cardiac fibrosis scores from trichrome-stained heart sections presented as mean ± S.D. with scatter plots of individual data points. (**D**) Wheat germ agglutinin (WGA) stain in left ventricle sections of 3 genotypes after 6-week Pi treatment. Upper panel is representative microscopic images of WGA stain from each treatment. Scale bar = 50 μm. Bottom panel is summary of data presented as mean ± S.D. with scatter plots of individual data points. Each treatment has 5 mice. (**E**) Immunoblots of total left ventricle lysates for α-actinin and α-SMA expression. Left panel is representative blots from each treatment. Right panel is summary data presented as mean ± S.D. with scatter plots of individual data points. Each treatment has 5 mice. *P<0.05, **P<0.01 between two groups by two-way ANOVA followed by Student-Newman-Keuls *post hoc* test for **A**, **C** - **E**.

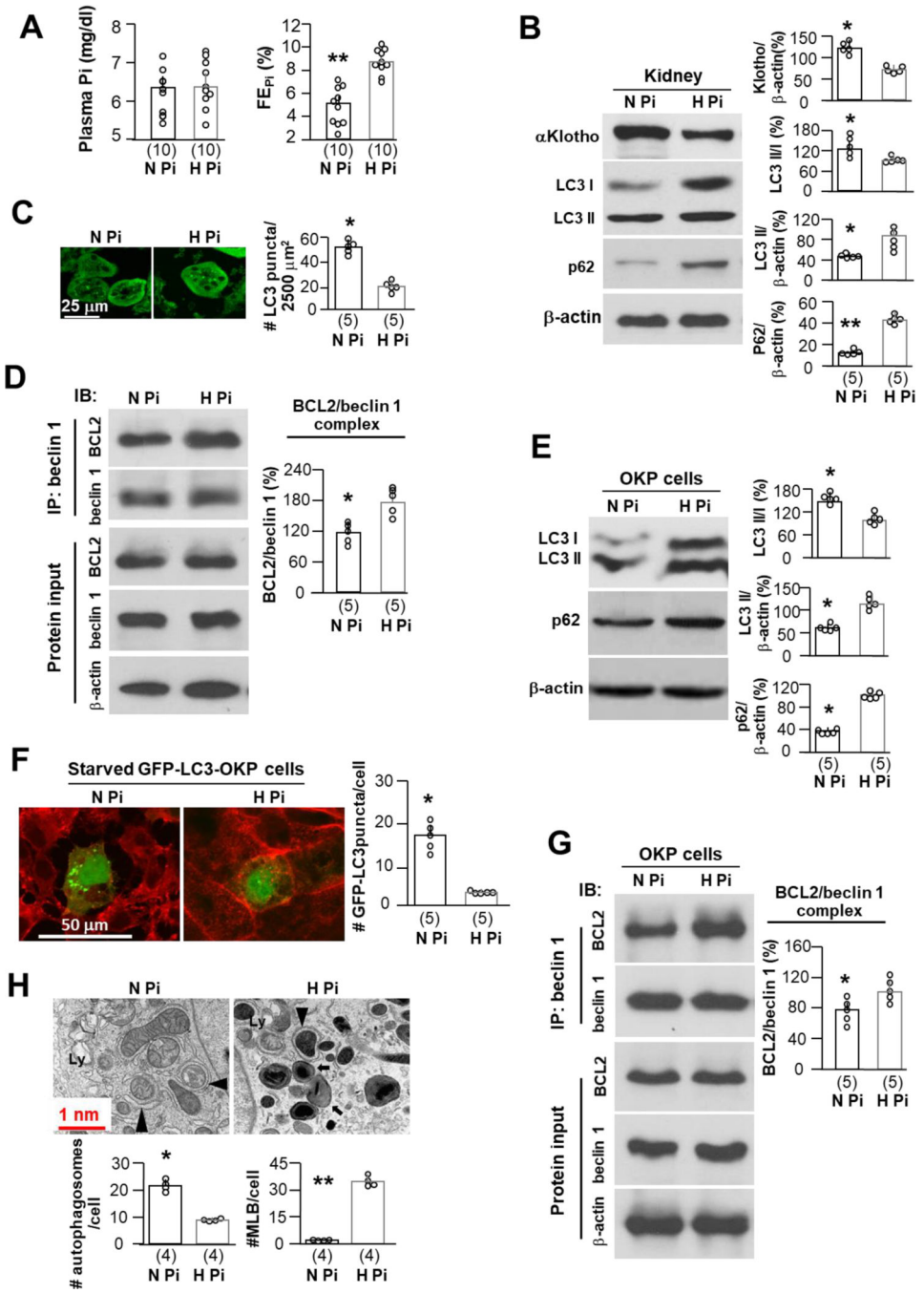

Fig. 7. High Pi decreases autophagy flux and downregulates αKlotho.

WT mice were fed with normal or high Pi diet starting at 10 weeks old for 2 weeks. (**A**) Plasma Pi (left panel) and fractional excretion of phosphate (FE_{Pi}) (right panel) after 2-week dietary Pi treatment. The data are presented as mean ± S.D. plus scatter plots. Each treatment has 10 mice. (**B**) Immunoblots of total kidney lysates for αKlotho, LC3 and p62 protein in the kidneys of mice from **A.** Left panel is representative immunoblots from each treatment. Right panel is summary of data from all of blots and presented as mean ± S.D. with scatter plots of individual data points. Each treatment has 5 mice. (**C**) Autophagic flux

in the kidneys of GFP-LC3 reporter mice treated normal or high Pi diet for 2 weeks starting at 10 weeks old. Each treatment has 5 mice. Four hours prior to sacrifice, mice were treated intraperitoneally with chloroquine treatment. Left panel is representative images of GFP-LC3 immunofluorescence in the renal tubules. Scale bars = 25 μm. Right panel summarizes quantitation of GFP-LC3 punctas in renal tubules. The data are presented as mean ± S.D. with scatter plots of individual data points. Each treatment has 5 mice. (**D**) Co-immunoprecipitation of beclin 1 and BCL2 in total kidney lysates from 5 mice presented in Figure 6B. Left upper panel shows representative immunoblots for Co-IP. Left bottom panel shows representative immunoblots from protein inputs. Right panel is a summary of co-IP data from 5 independent experiments. Data are presented as mean ± S.D. with scatter plots of individual data points. (**E**) OKP cells were treated normal Pi (0.96 mM) or high Pi (3.0 mM) media. At 24 hours, cells were harvested. Autophagic flux in OKP cells treated with normal or high Pi media is evaluated. Left panel shows representative immunoblots of total cell lysates for LC3 and p62 protein from 5 independent experiments. Right panel summarizes the data presented as mean ± S.D. with scatter plots of individual data points. (**F**) OKP cells were transiently transfected with GFP-LC3 plasmid and 48 hours later were treated with normal Pi or high Pi media for 24 hours. Left panel shows representative images of GFP-LC3 immunofluorescence from 5 independent experiments. Right panel is the summary of quantitative data of LC3 punctas presented as mean ± S.D. with scatter plots of individual data points. Scale bars = 50 μm. (**G**) Co-immunoprecipitation of beclin 1 and BCL2 in total cell lysates from Figure 6E. Left upper panel shows representative immunoblots for Co-IP. Left bottom panel shows representative immunoblots from protein inputs. Right panel is a summary of co-IP data from 5 independent experiments. Data are presented as mean ± S.D. with scatter plots of individual data points. (**H**) Autophagic ultramicroscopic structures in OKP cells treated with normal or high Pi media descripted in Figure 6E. Upper panel is representative electronic microscopic images showing autophagosomes (arrow head) and autolysosomes (Ly) and multilamellar bodies (MLB) (arrow). Scale bars = 1.0 nm. Bottom panels are summaries of autophagosomes and MLB per cell from total 25 cells of normal (N Pi) or high Pi (H Pi) treatment from 4 independent experiments. The data were presented as mean ± S.D. with scatter plots of individual data points. *P<0.05; **P<0.01 between 2 groups by unpaired *t*-test for **A**-**C**, **E**, **F**, and **H**.

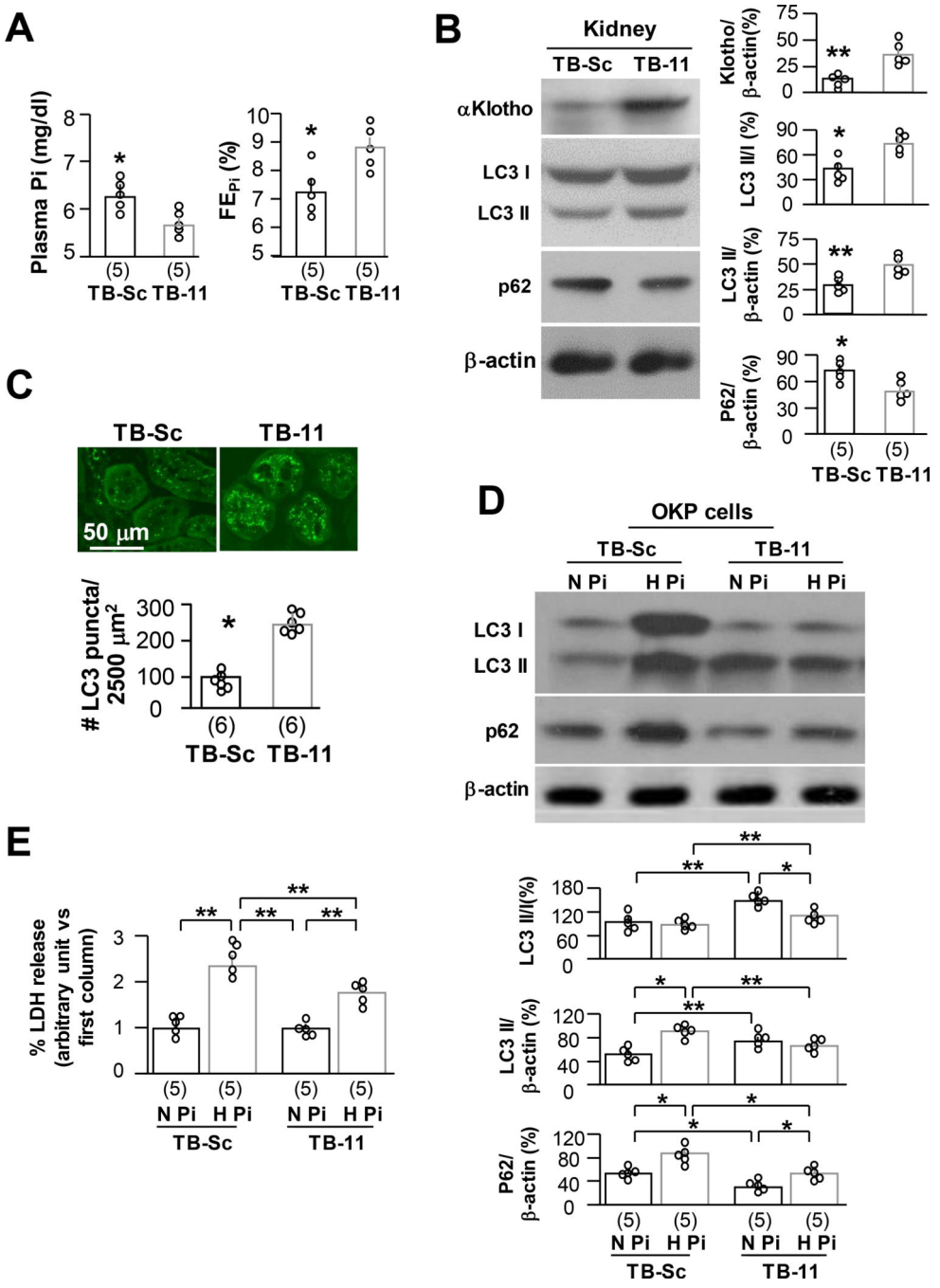

Fig. 8. Tat-beclin 1 peptide upregulates autophagy flux and protects against phosphotoxicity in renal proximal tubular cells.

GFP-LC3 reporter (*LC3*) mice at 10 weeks-old were intraperitoneally injected TB-11 or TB-Sc (2 mg/kg daily for 4 weeks). Four hours prior to sacrifice, mice were intraperitoneally injected chloroquine (**A-C**). Each treatment consisted of 5 mice. (**A**) Plasma Pi (left panel) and fractional excretion of phosphate (FE_{Pi}) (right panel) of *LC3* mice. The data is presented at mean ± S.D. with scatter plots of individual data points. (**B**) Immunoblots for αKlotho, LC3, p62, and β-actin protein in the kidneys. Left panel shows representative immunoblots.

Right panel is quantitation of all blots from each treatment. (**C**) Autophagic flux in the kidneys of *LC3* mice. Each treatment has 5 mice. Upper panel is representative images of GFP-LC3 immunofluorescence in the renal tubules. Scale bars = 50 μm. Bottom panel summarizes quantitation of GFP-LC3 punctas in renal tubules. The data are presented as mean ± S.D. with scatter plots of individual data points. *P<0.05; **P<0.01 between 2 groups by unpaired *t*-test for **A**-**C**. TB-11 or TB-Sc (10 μM for 24 hours) were added to OKP cells with normal (0.96 mM) or high (3.0 mM) Pi (**D** and **E**). (**D**) Immunoblots of total cell lysates for LC3 and p62 protein in the OKP cells. Upper panel is representative immunoblots from each treatment. Bottom panel is summary of data from all of blots. (**E**) LDH in culture media. Data are presented as mean ± S.D. with scatter plots of individual data points from 5 independent experiments. *P<0.05; **P<0.01 between 2 groups by two-way ANOVA for **D** and **E**.

Table 1.

Effect of high Pi diet on plasma αKlotho, cFGF23, and 1,25-$(OH)_2$D

		αKlotho (pmol/l)	cFGF23 (RU/ml)	1,25-$(OH)_2$D (pg/ml)
Normal Pi diet				
	WT	45.6±3.5 (14)	105.7±28.2 (12)	104.5±13.4 (14)
	BK/BK	48.7±4.1 (14)	139.5±26.4 (12)	96.5±4.6 (12)
	BK/BK;kl/kl	41.2±3.5 (12)	144.5±32.3 (14)	113.4±12.5 (14)
	P value	>0.05	>0.05	>0.05
High Pi diet				
	WT	31.1±2.3 (14)	347.4±35.0 (14)	277.2±31.6 (16)
	BK/BK	42.2±3.3** (16)	353.6±45.6 (12)	124.2±21.4** (14)
	BK/BK;kl/kl	30.2±3.0## (10)	431.7±84.3*# (10)	347.4±42.1**## (10)
	P value	<0.01	<0.05	<0.01

Three mouse lines (*WT*, *BK/BK*, and *BK/BK;kl/kl*) were fed with normal Pi (0.7%) or high Pi (2.0%) diet for 6 weeks starting at 6 weeks old. The ratio of female and male mice were 50:50. After 6 weeks of dietary Pi challenge, mice were terminated and plasma was harvested for the measurement of soluble αKlotho, C-terminal FGF23, and 1,25-$(OH)_2$D. Data are presented as means ± S.D., the number in parentheses is sample size. The statistical analysis was conducted with one-way ANOVA followed by post hoc tests for any two groups.

* P<0.05

** P<0.01 vs *WT* mice

\# P<0.05

\#\# P<0.01 vs *BK/BK* mice by one-way ANOVA followed by Student-Newman-Keuls *post hoc* test. cFGF23: c-terminal fragments of fibroblast growth factor-23; *kl/kl:* homozygous αKlotho hypomorphs; Pi: inorganic phosphate; 1,25-$(OH)_2$D: 1,25-dihydroxyl-vitamin D; *WT*: wild type.